Journal Pre-proof

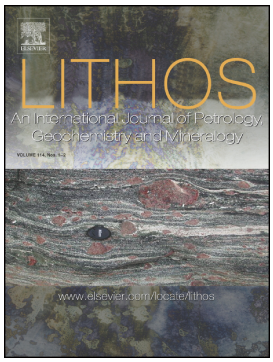

Melting and metasomatism/refertilisation processes in the Patagonian sub-continental lithospheric mantle: A review

Massimiliano Melchiorre, Barbara Faccini, Michel Gregoire, Mathieu Benoit, Federico Casetta, Massimo Coltorti

PII: S0024-4937(19)30484-0

DOI: https://doi.org/10.1016/j.lithos.2019.105324

Reference: LITHOS 105324

To appear in: *LITHOS*

Received date: 10 April 2019

Revised date: 26 November 2019

Accepted date: 4 December 2019

Please cite this article as: M. Melchiorre, B. Faccini, M. Gregoire, et al., Melting and metasomatism/refertilisation processes in the Patagonian sub-continental lithospheric mantle: A review, *LITHOS*(2019), https://doi.org/10.1016/j.lithos.2019.105324

Melting and metasomatism/refertilisation processes in the Patagonian Sub-Continental Lithospheric Mantle: a review

Massimiliano Melchiorre[a,b], Barbara Faccini[b*], Michel Gregoire[c], Mathieu Benoit[c], Federico Casetta[b], Massimo Coltorti[b]

[a] Institute of Earth Sciences Jaume Almera, CSIC, Carrer Luís Solé i Sabarís s/n, 08028 Barcelona, Spain.

[b] Department of Physics and Earth Sciences, University of Ferrara, Via Saragat 1, 44121 Ferrara, Italy.

[c] Géosciences Environnement Toulouse, Université de Toulouse; UPS OMP-CNRS-IRD, 14 Avenue E. Belin, 31400 Toulouse, France.

*Corresponding author: Barbara Faccini, Department of Physics and Earth Sciences, University of Ferrara, Via Saragat 1, 44121 Ferrara, Italy. *E-mail address:* barbara.faccini@unife.it

Melting and metasomatism/refertilisation processes in the Patagonian Sub-Continental Lithospheric Mantle: a review

Abstract

The large amount of geochemical variability in peridotitic and pyroxenitic xenoliths exhumed by Eocene to present-day magmas in Patagonia provides a unique opportunity to investigate the depletion and enrichment processes affecting the lithosphere in proximity of subduction settings and their relationships with magmatism. In this study, a review of the geochemical features of the Patagonian ultramafic xenoliths coupled with new Sr-Nd isotopic data on clinopyroxene separates from representative suites enabled us to delineate the main melt extraction and enrichment (metasomatism vs. refertilisation) processes acting in these sub-continental lithospheric mantle (SCLM) portions. Our findings show that clinopyroxenes and orthopyroxenes in Patagonian harzburgites/lherzolites lie on two discrete Al_2O_3/MgO trends and record variable partial melting degrees (1-30%), progressively decreasing southward, where the mantle domains experienced melt extraction in the past. The occurrence of both negative and positive correlations between $(La/Yb)_N$, Sr_N, and Al_2O_3 in clinopyroxenes suggests that large part of the SCLM beneath Patagonia was affected by both metasomatic (low melt-fluid/rock ratio) and refertilisation (high melt-fluid/rock ratio or long-lasting low melt-fluid/rock interaction) processes, while a few portions - particularly in Southern Patagonia - were devoid of significant enrichment processes. A comprehensive study of the major/trace element composition and rare earth element patterns of clinopyroxene from both cumulitic and mantle xenoliths led us to hypothesize that tholeiitic enrichment was followed by infiltration of transitional/alkaline agents in the Northern and Central Patagonian SCLM. The percolation of melts with transitional affinity can be identified in some Central Patagonian localities. In Southern Patagonia clinopyroxenes record a slight interaction with alkaline and proto-adakitic agents; the latter occurred at Cerro Fraile, the locality nearest the trench. The Sr-Nd xenolith isotopic signature led to speculation that enriched and depleted mantle components interacted variably in the SCLM domain beneath Patagonia. This work suggests that a detailed and comprehensive study of

ultramafic xenoliths can help identify the evidence produced by magmatic events occurring at the surface, as both a serial affinity and a temporal sequence.

Keywords: Patagonia, Sub-Continental Lithospheric Mantle, alkaline metasomatism, tholeiitic refertilisation

1. Introduction

The mantle xenoliths brought to the surface in the proximity of subduction settings are a powerful tool to investigate the depletion and enrichment processes affecting the lithospheric mantle. The dehydration of the subducting slab can lower the melting point of the overlying mantle wedge and trigger melt extraction (depletion processes). Enrichment processes are instead ascribed to the release of fluids/melts that modify the chemical composition of the mantle by adding incompatible elements (in some cases changing the major element budget as well) and eventually affecting its isotopic composition. Once transported to the surface, mantle xenoliths can signal these depletion and/or enrichment processes; the former are related to partial melting and the latter to both metasomatic and refertilisation events. Patagonia is a key locality for investigating depletion/enrichment processes affecting the mantle wedge in the proximity of a subducting slab. Throughout the entire Patagonian region, from the Eocene to the present, plateau magmatism with tholeiitic to transitional/alkaline affinity transported large amounts of peridotitic and pyroxenitic xenoliths from the underlying lithosphere to the surface (Fig. 1). The large geochemical variability of these xenoliths provides evidence for moderate to strong depletion events (up to 30% partial melting) affecting the sub-continental lithospheric mantle (SCLM) wedge beneath Patagonia and for subsequent variable metasomatic/refertilisation processes (Aliani et al., 2009; Bjerg et al., 2005, 2009; Conceicao et al., 2005; Dantas, 2007; Dantas et al., 2009; Faccini et al., 2013; Gorring and Kay, 2000; Kilian and Stern, 2002; Laurora et al., 2001; Melchiorre et al., 2015; Mundl et al., 2015, 2016; Ntaflos et al., 2007; Rivalenti et al., 2004, 2007; Schilling et al., 2005, 2008, 2017; Stern et al., 1999). Nevertheless,

the nature and provenance of fluids/melts pervading this mantle wedge is still debated, while a comprehensive model of the depletion and enrichment processes affecting the Patagonian SCLM is still far from settled.

In some localities, the interaction between slab-derived fluids and previously depleted mantle domains is evidenced by the presence of modal amphibole and phlogopite (Comallo and Gobernador Gregores, n. 6 and 20 in Fig. 1, respectively; Laurora et al., 2001; Mundl et al., 2016). The occurrence of slab-derived melts has been proposed at Cerro Fraile (n. 23 in Fig. 1) by Kilian and Stern (2002), who related the high Sr/Y, La/Yb, and La/Nb ratios of the mantle xenoliths to the infiltration of high-Mg#, low-Y adakitic melts similar in composition to those in the neighbouring Austral Volcanic Zone. Further support for this hypothesis was provided by Faccini et al. (2013) who ascribed the enrichment in Zr, Th, and U of pyroxenes from Cerro Fraile xenoliths to the slab melting of Mn nodules and organic-rich sediments present on the ocean floor of the Antarctic Plate.

In some localities (Prahuaniyeu, n. 8 in Fig. 1) the low Ti/Nb and high Zr/Hf ratios of spinel-bearing peridotites promote the percolation of carbonatitic melts through the Patagonian lithosphere (Bjerg et al., 2009). The occurrence of carbonatitic metasomatism was also invoked for some xenoliths from Estancia Lote 17 (Gobernador Gregores, n. 20 in Fig. 1; Gorring and Kay, 2000), even though Aliani et al. (2009) recently dismissed a mantle origin for such occurrence, suggesting that at least part of the carbonate was introduced to the xenoliths by percolating meteoric water.

Negative correlations between $(La/Yb)_N$ and Al_2O_3 and between Sr_N and Al_2O_3 in clinopyroxenes, together with the presence of orthopyroxenitic veins, led Melchiorre et al. (2015) to hypothesize that a refertilisation event triggered by transitional alkaline/sub-alkaline melts occurred in the SCLM beneath Estancia Sol de Mayo (n. 16 in Fig. 1).

In some localities mantle xenoliths devoid of any significant metasomatic imprint were also documented, as in the case of Tres Lagos (n. 22 in Fig. 1), where a suite of nodules record only partial melting events in the garnet and spinel stability fields (Ntaflos et al., 2007).

Mundl et al. (2015, 2016) and Schilling et al. (2017) proposed the existence of multiple discrete SCLM domains with different depletion ages beneath Patagonia based on Re-Os systematics. According to these authors, the mantle domain beneath Pali Aike (n. 25 in Fig. 1) yields the oldest depletion ages (up to 2.5 Ga), whereas the SCLM beneath the northern localities are characterized by younger ages varying between 0.5 and 1.0 Ga.

In the present study, a review of the main geochemical features of several Patagonia mantle xenolith suites, strengthened by new Sr-Nd isotopic analyses of clinopyroxene separates from representative localities, is advanced. Main goals are to: i) investigate (and discriminate between) metasomatism and refertilisation processes affecting the mantle domains; ii) constrain the nature of the melt/fluid circulating in the Patagonian SCLM; iii) evaluate the possible interactions among different mantle reservoirs and iv) identify the presence (if any) of large-scale depletion/enrichment processes in the SCLM beneath Patagonia.

A further consideration concerns the type of chemical modification of the mantle, namely, if the enrichment process is related to a metasomatic (either cryptic or modal) or a refertilisation event. The term metasomatism defines the sub-solidus modification of a rock's chemical composition, through invasive percolation of/reaction with liquids. If the original solid-solution phase assemblage remains the same but changes in composition, metasomatism is defined as "cryptic", whereas if new phases are added to the pristine mineral paragenesis, the metasomatism is defined as "modal" (O'Reilly and Griffin, 2013). On the other hand, a refertilisation event is identified when a previously depleted peridotitic rock is impregnated by percolating melts that are able to impart a new and usually more fertile mineralogical and chemical composition (Le Roux et al., 2007; Pelorosso et al., 2016). This case can be identified with the concept of "stealth" metasomatism introduced by O'Reilly and Griffin (2013), who highlighted the difficulty in identifying the eventual enrichment process when it ends with a mineralogical/chemical composition comparable to that of the starting fertile mantle.

Under the assumption that the processes of metasomatism and refertilisation are essentially related to different melt/rock ratios, in this work we speculate about the different effects that these processes may have had on the peridotitic matrix in various localities throughout Patagonia.

2. Geological setting

Patagonia is the continental region of South America lying south of the Huincul Fault (Ramos et al., 2004; Schilling et al., 2017). It extends from ~39° and ~54° S between the Southern and Austral Volcanic Zones (the SVZ and AVZ, respectively), the two southernmost portions of the Andean Cordillera (Stern and Kilian, 1996). The subduction of the Chile Ridge beneath the South American Plate, occurring in conjunction with the so-called Triple Junction (46.3° S; Cande and Leslie, 1986), marks the separation between SVZ and AVZ and is reflected by a gap in the volcanism from 46 to 49° S (D'Orazio et al., 2000; Fig. 1).

Patagonia consists of three geographical provinces (Rio Negro, Chubut, and Santa Cruz) and is characterized by the presence of several Eocene to Holocene volcanic plateaus located behind the Andean arc chain (Fig. 1; see Kay et al., 2004; Ramos and Kay, 1992). These plateaus, composed of transitional to alkaline lavas, generally developed in three evolutionary stages: "pre-plateau", "main plateau", and "post-plateau", the second being the most voluminous. The Somoncura Volcanic Field (Fig. 1) is considered the largest post-Eocene mafic volcanic field within Patagonia (Kay et al., 2007). It consists of a series of Oligocene to early Miocene volcanic fields covering more than 55,000 km^2 in the Meseta de Somoncura and surrounding regions (Meseta de Cari Laufquen and Meseta de Canquel). It overlies Cretaceous to early Tertiary volcanic and sedimentary rocks (Ardolino et al., 1999; Rapela and Kay, 1988; Rapela et al., 1988), the extensive Jurassic silicic volcanic rocks of the Chon Aike Province (Kay et al., 1989; Pankhurst and Rapela, 1995), and a late Precambrian to Palaeozoic magmatic and metamorphic basement. The unique geodynamic setting of the volcanic gap region, related to the Middle Eocene to present northward migration of the Chile Triple Junction (from ~49° S to 46.3° S; Cande and Leslie, 1986), resulted in extensive Late Miocene to Pleistocene

magma production. The volcanic activity of the southern portions of Patagonia consists of a voluminous, tholeiitic to transitional Late Miocene to Early Pliocene main plateau sequence (Meseta de la Muerte, Belgrano, Central, and Lago Buenos Aires) and of a less voluminous, transitional to alkaline late Miocene to Plio-Pleistocene post-plateau sequence (Gorring et al., 1997). The youngest (Pliocene to present) Patagonian lava flows constitute the Pali Aike Volcanic Field (49-52° S; Stern et al., 1989), a 4,500-km^2 succession of alkaline basaltic lava flows and subordinated monogenetic structures such as maars, tuff-rings, scoria, and spatter cones (D'Orazio et al., 2000). These small volcanic centres are aligned ENE-WSW and NW-SE, and are probably linked to the still-active Magallanes Strait Rift System (Diraison et al., 1997) and to the Mesozoic Patagonian Austral Rift (Corbella et al., 1996), respectively.

Most of the Eocene to present plateau lavas brought considerable quantities of mantle xenoliths to the surface, mainly peridotitic in composition, with less abundant pyroxenites. A summary of the known Patagonian xenolith-bearing localities is reported in Fig. 1 (see Aliani et al., 2009; Bjerg et al., 2005, 2009; Conceicao et al., 2005; Dantas, 2007; Dantas et al., 2009; Faccini et al., 2013; Gorring and Kay, 2000; Kilian and Stern, 2002; Laurora et al., 2001; Melchiorre et al., 2015; Mundl et al., 2015, 2016; Ntaflos et al., 2007; Rivalenti et al., 2004, 2007; Schilling et al., 2005, 2008, 2017; Stern et al., 1999).

According to Bjerg et al. (2009), Dantas (2007), Dantas et al. (2009), Folguera et al. (2018), Kay et al. (2013), Melchiorre et al. (2015), and Rivalenti et al. (2004), Patagonia can be subdivided into three main sectors: Northern (39/40-46° S), Central (46-49° S), and Southern (49-54° S). Such a subdivision is particularly effective to emphasize the features of the Central Patagonian mantle region, which experienced Middle Eocene to present interactions with the subducting Chile Ridge (Cande and Leslie, 1986; Folguera et al., 2018). Further support to this discrimination is given by the (few) ages reported for the xenolith-bearing volcanic products (basaltic necks, cinder cones, scoria cones, and maars) in the literature; these are generally younger moving southwards. The xenolith-bearing volcanic products located north of the Chile Triple Junction were, in fact, emplaced after 61 Ma;

those from Central and Southern Patagonia are younger than 42 and 7 Ma, respectively (see Bjerg et al., 2005; Dantas, 2007; Dantas et al., 2009; Melchiorre et al., 2015; Mundl et al., 2015; 2016; Schilling et al., 2017). In this framework, we consider the following localities as belonging to Northern Patagonia (Fig. 1): Laguna Fria (1), Cerro Chenque (2), Puesto Diaz (3), Estancia Alvarez (4), Cerro Aznares (5), Comallo (6), Cerro Mojon (7), Prahuaniyeu (8), Traful (9), Cerro Rio Chubut (10), Paso de los Indios (11), Cerro de los Chenques (12), and Coyhaique (13). Central Patagonia is represented by Chile Chico (14), Cerro Clark (15), Estancia Sol de Mayo (16), Don Camilo (17), Cerro Cuadrado (18), Auvernia (19), Gobernador Gregores + Estancia Lote 17 (20), and Cerro Redondo (21). Southern Patagonia includes Tres Lagos (22), Cerro Fraile (23), Las Cumbres (24), and Pali Aike (25).

3. Sample localities and analytical methods

$^{87}Sr/^{86}Sr$ and $^{143}Nd/^{144}Nd$ isotopic measurements were performed on clinopyroxene separates from 29 samples from 7 Patagonian localities, thought to be representative of the SCLM beneath the Northern, Central, and Southern regions comprising Cerro Rio Chubut (n. 10 in Fig. 1), Cerro de los Chenques (n. 12 in Fig. 1), Cerro Clark (n. 15 in Fig. 1), Estancia Sol de Mayo (n. 16 in Fig. 1), Gobernador Gregores (n. 20 in Fig. 1), Cerro Fraile (n. 23 in Fig. 1), and Pali Aike (n. 25 in Fig. 1). A summary of the petrographic features of the analysed samples is given in Appendix A, whereas major/trace element analyses of selected clinopyroxenes from the above localities (Table 1) are reported by Aliani et al. (2009), Dantas (2007), Dantas et al. (2009), Faccini et al. (2013), and Melchiorre et al. (2015). $^{87}Sr/^{86}Sr$ and $^{143}Nd/^{144}Nd$ were measured with a thermal ionization mass spectrometer (TIMS) at the UMR 5563 (GET, Observatoire Midi-Pyrenees) of the University Paul Sabatiér (Toulouse III). Measurements of Sr and Nd isotopic ratios were realized on leached hand-picked clinopyroxenes, following the method described in Snow et al. (1994) and used in Benoit et al. (1999), to reduce the effect of the hydrothermal fluid-rock interactions, which mainly affect the $^{87}Sr/^{86}Sr$ ratios. Leached clinopyroxenes underwent acid digestion with a mixture of $HF–HClO_4$ at

140 °C, to prevent the formation of Ca fluorides, which trap rare earth elements (REE). Sample drying was done at the same temperature until the complete evaporation of $HClO_4$. Chemical separation was performed on combined Sr-Spec/Thru-Spec columns. The Sr cut was processed again through the same column to efficiently separate Sr from Rb and Ca, while Nd was further eluted on LnSpec Eichrom resin. Isotopic measurements were conducted on a Finnigan Mat 261 mass spectrometer. Sr was run on a single W filament with Ta activator, while Nd was run on a Re double filament. The NBS 987 (for Sr) and La Jolla (for Nd) standards were run regularly to check the measurements: the average value of $^{87}Sr/^{86}Sr = 0.710248 \pm 0.000020$ (n = 17), average value $^{87}Sr/^{86}Sr = 0.710246 \pm 0.000012$ (n = 23), and average value $^{143}Nd/^{144}Nd = 0.511853 \pm 0.000010$ (n = 16). Blanks were < 650 pg for Sr and < 350 pg for Nd.

4. Clinopyroxene, orthopyroxene and olivine chemistry

4.1. Summary of previously published data

Clinopyroxenes from Northern, Central and Southern Patagonia mantle xenoliths depict steep trends characterized by a Mg# [calculated as $Mg/(Mg+Fe^{2+})$ mol%, by considering all Fe as Fe^{2+}] increase coupled with an Al_2O_3 content decrease (Fig. 2). Clinopyroxenes from Northern Patagonia harzburgites and lherzolites have Mg# varying between 88.3 and 95.0, with Al_2O_3 ranging from 8.0 to 1.7 wt.%, showing a good linear correlation (Fig. 2a). The distribution of Al_2O_3 vs. Mg# in clinopyroxenes from Central Patagonian harzburgites and lherzolites is scattered, notwithstanding similar compositional ranges (Mg# 87.9-94.4; Al_2O_3 1.8-7.1 wt.%; Fig. 2b). The case of clinopyroxenes in Southern Patagonia harzburgites and lherzolites (Fig. 2c) is slightly different, exhibiting substantially lower Al_2O_3 content (0.6-6.8 wt.%) at comparable Mg# (88.4-94.1).

Clinopyroxenes from Northern Patagonia dunites and websterites (Fig. 2d) plot on two discrete trends, one of which is comparable to that of harzburgites and lherzolites (Mg# 89.1-92.7; Al_2O_3 3.8-7.5 wt.%) whereas the other is typified by a lower Al_2O_3/Mg# ratio (Mg# 83.9-89.8; Al_2O_3 2.6-5.2 wt.%). Clinopyroxenes in Central Patagonian dunites, wehrlites, websterites, and clinopyroxenites

(Fig. 2e) have similar features, as demonstrated by the presence of two trends with high and low Al_2O_3/Mg# ratios (Mg# 89.5-92.9 and Al_2O_3 4.0-7.2 wt.% the former; Mg# 81.6-90.2 and Al_2O_3 2.3-6.4 wt.% the latter). Finally, clinopyroxenes in Southern Patagonian dunites, orthopyroxenites, and clinopyroxenites (Fig. 2f) plot mainly on a low Al_2O_3/Mg# trend (Mg# 83.7-94.1; Al_2O_3 1.4-4.0 wt.%), even though some samples are typified by a higher Al_2O_3 content (3.7-8.8 wt.%) in a narrower Mg# interval (90.9-92.9).

Orthopyroxenes from Northern, Central, and Southern Patagonia harzburgites and lherzolites (Fig. 3) have features similar to the coexisting clinopyroxenes. Orthopyroxenes from Northern Patagonia are characterized by Mg# varying between 88.0 and 93.7 and Al_2O_3 between 0.7 and 6.1 wt.%, which is quite comparable to those from Central Patagonian xenoliths (Mg# 87.5-93.0 and Al_2O_3 0.1-6.3 wt.%). With respect to their clinopyroxenes, which are aligned on a single Al_2O_3 vs. Mg# trend, orthopyroxenes from Northern Patagonia lie on two discrete trends; one of these, typified by lower Al_2O_3/Mg# ratio, is represented mainly by Cerro Aznares harzburgites (Fig. 3a). Analogous considerations can be made for Central Patagonia, where a low Al_2O_3/Mg# trend mostly typifies orthopyroxenes in Estancia Sol de Mayo harzburgites and lherzolites (Fig. 3b). Southern Patagonian orthopyroxenes behave similarly to the coexisting clinopyroxenes, with a Mg# of 87.3-92.2 and Al_2O_3 mostly ranging between 2.0 and 4.6 wt.%. An exception is seen in some Tres Lagos samples, in which orthopyroxene reaches Al_2O_3 contents up to 5.8 wt.% (Fig. 3c). Clinopyroxene and orthopyroxene from Northern Patagonia dunites and websterites (Fig. 3d) lie on two discrete trends, typified by lower and higher Al_2O_3/Mg# ratios (Mg# 80.4-88.3 and Al_2O_3 1.2-3.6 wt.% and Mg# 89.8-91.6 and Al_2O_3 3.4-4.6 wt.%, respectively). Orthopyroxenes from Central Patagonian dunites, wehrlites, websterites, and clinopyroxenites (Fig. 3e) have similar features except for the wider Al_2O_3 interval (from 1.6 up to 5.9 wt.%). In addition, orthopyroxenes from Southern Patagonian dunites and orthopyroxenites (Fig. 3f) can be subdivided into two distinct groups with different Al_2O_3/Mg# ratios (Mg# 80.7-88.0 and Al_2O_3 2.0-4.6 wt.% and Mg# 89.8-90.7 and Al_2O_3 2.4-3.6 wt.%, respectively).

Likewise pyroxenes, olivine from Northern and Central Patagonia harzburgites/lherzolites is characterized by similar composition, with forsterite (Fo) content ranging from 89.2 to 91.9 and from 88.1 to 92.0, respectively. NiO content ranges between 0.26 and 0.50 wt.% in both Northern and Central Patagonia samples. Olivine from Southern Patagonia localities is characterized by a narrower Fo interval (88.0-91.3) and a wider NiO range (0.27-0.57 wt.%; Fig. 4).

Olivines in Northern Patagonia dunites and websterites are generally similar to those from harzburgites and lherzolites (Fo 89-90; NiO 0.32-0.4 wt.%; Fig. 4a), except for a few crystals, which are characterized by lower Fo (~86) at comparable NiO content (0.30-0.32 wt.%). A complete overlap between harzburgites/lherzolites and dunites, wehrlites, and websterites is shown in Central Patagonian olivines, which have Fo 89-91 at NiO ranging between 0.21 and 0.45 wt.% (Fig. 4b). Olivine from Southern Patagonia dunites and orthopyroxenites are generally less magnesian that those from harzburgites/lherzolites, having Fo between 86 and 90 and NiO comprised between 0.28 and 0.44 wt.% (Fig. 4c).

To estimate the depletion and enrichment processes (melt extraction and metasomatism) that occurred in the SCLM beneath Patagonia, a comparison between trace element concentration and Al_2O_3 content of clinopyroxene in both peridotitic and pyroxenitic xenoliths was performed. In Fig. 5, the behaviour of chondrite-normalized (Sun and McDonough, 1989) La/Yb ratio and Sr (hereafter $(La/Yb)_N$ and Sr_N, respectively) in clinopyroxenes is correlated to their Al_2O_3 content.

A group of clinopyroxenes is characterized by light rare earth elements (LREE) enrichment (increase in the $(La/Yb)_N$ ratio) coupled with Al_2O_3 depletion (Fig. 5a). This behaviour is observable in Northern, Central, and Southern Patagonia localities (Cerro Mojon, Prahuaniyeu, Paso de los Indios, Cerro de los Chenques, Don Camilo, Estancia Sol de Mayo, Cerro Fraile, and Pali Aike). However, a positive correlation between LREE and Al_2O_3 content is displayed by clinopyroxenes from Cerro Rio Chubut and Gobernador Gregores (Fig. 5b), although some samples from these localities "flatten" at around $(La/Yb)_N = 10$. Some localities do not display a clear correlation between LREE and Al_2O_3: this is the case of Estancia Alvarez, Cerro Aznares, Cerro Chenque, Puesto Diaz, Comallo, Cerro

Clark, Cero Cuadrado, Tres Lagos and Las Cumbres (Fig. 5c). A general correspondence between Sr_N and $(La/Yb)_N$ vs. Al_2O_3 diagrams could be observed, notwithstanding that the Sr_N trends are less marked than the $(La/Yb)_N$ ones (Fig. 5d-e-f). Exceptions are constituted by few localities from Northern and Southern Patagonia (Cerro Aznares, Cerro Chenque, Puesto Diaz, Comallo, and Tres Lagos) - which show a positive correlation between Sr_N and Al_2O_3 but a scattered REE distribution - and by Cerro Fraile, where there is no correlation between Sr_N and Al_2O_3.

4.2. Results: Sr-Nd isotopes

The new Sr-Nd isotopic compositions of clinopyroxene separates from 29 Patagonia xenoliths are reported in Table 1 and Fig. 6. All samples are aligned along the mantle array (DePaolo and Wasserburg, 1979) and are characterized by $^{87}Sr/^{86}Sr$ ranging from 0.7027 to 0.7043 and by $^{143}Nd/^{144}Nd$ between 0.51269 and 0.51309. Clinopyroxenes from Cerro Rio Chubut and Estancia Sol de Mayo lie on a narrow interval, characterized by a high Sr isotopic signature ($^{87}Sr/^{86}Sr$ from 0.7037 to 0.7039; $^{143}Nd/^{144}Nd$ from 0.51269 to 0.51279). Cerro Fraile, Gobernador Gregores and Pali Aike clinopyroxenes have similar Sr-Nd isotopic signatures, with $^{87}Sr/^{86}Sr$ generally falling between 0.7030 and 0.7035 and $^{143}Nd/^{144}Nd$ in the range 0.51281-0.51299. The Sr-Nd isotopic range of Cerro de los Chenques and Cerro Clark clinopyroxenes is wider, covering the entire $^{87}Sr/^{86}Sr$ and $^{143}Nd/^{144}Nd$ interval (Fig. 6).

The Sr-Nd isotopic signature of all the analysed samples is comparable to that of clinopyroxene separates from other Patagonian localities (Bjerg et al., 2009; Gorring and Kay, 2000; Mundl et al., 2015, 2016; Rivalenti et al., 2007; Fig. 6), lying between the depleted mantle (DMM; Workman and Hart, 2005) and the enriched mantle end-members (EM I, Zindler and Hart, 1986; EM II, Hart, 1988). No systematic variations in the $^{87}Sr/^{86}Sr$ and $^{143}Nd/^{144}Nd$ ratios between Northern, Central, and Southern Patagonia xenoliths were identified (Fig. 6), even though Gobernador Gregores, Cerro Fraile and Pali Aike samples have similar signatures, which are generally more depleted than the rest of the Central Patagonia samples (Cerro Clark and Estancia Sol de Mayo). The correlation between

the analysed samples and the compositional fields of Northern, Central and Southern Patagonia mantle xenoliths reported in literature (Bjerg et al., 2009; Gorring and Kay, 2000; Mundl et al., 2015, 2016; Rivalenti et al., 2007) is total (Fig. 6). Overall, a wider Sr-Nd isotopic range characterizes Central and Southern Patagonia ($^{87}Sr/^{86}Sr$ = 0.7023-0.7059; $^{143}Nd/^{144}Nd$ = 0.51223-0.51328) with respect to Northern Patagonia ($^{87}Sr/^{86}Sr$ = 0.7027-0.7048; $^{143}Nd/^{144}Nd$ = 0.51262-0.51313).

5. Depletion and enrichment processes beneath Patagonia

In the following sections, a compilation of previously published data has been used to model and review the depletion and enrichment (metasomatism and refertilization) processes acting throughout the Northern, Central and Southern Patagonian SCLM. To obtain comparable results, the extent of depletion was evaluated by applying major/trace element melting models to orthopyroxene and clinopyroxene (Bonadiman and Coltorti, 2011; Upton et al., 2011; Zou, 1998) from harzburgites and lherzolites. Analogously, common criteria were adopted to estimate the enrichment processes recorded by clinopyroxene (see below). A summary of the compositional features of the xenoliths and a list of the obtained results are given in Table 2.

5.1. Melt extraction processes

The extent of depletion events related to melt extraction was estimated through the major element (MgO and Al_2O_3) composition of orthopyroxene and clinopyroxene (Bonadiman and Coltorti, 2011; Upton et al., 2011) and the trace element (Y and Yb) concentration of clinopyroxene (Zou, 1998). All these models work in the spinel stability field; therefore, the garnet-bearing harzburgites and lherzolites documented in two Patagonian localities (Prahuaniyeu and Pali Aike; Bjerg et al., 2009) were not taken into account. For these localities, only the spinel-bearing lithotypes were considered to model the depletion processes affecting these SCLM domains. In those samples where the amount of melt extraction recorded by orthopyroxene exceeded 25%, clinopyroxene was not considered to estimate the degree of melt extraction. Indeed, its presence in mantle residua after 25% partial melting

is unlikely (Scott et al., 2016; Walter, 2003) and the coexistence between Mg-rich orthopyroxene and clinopyroxene in some samples may be the result of subsequent metasomatic/refertilisation processes.

5.1.1. Depletion processes modelled through major elements

In Fig. 7 the Al_2O_3 content of orthopyroxene from Northern, Central, and Southern Patagonia harzburgites and lherzolites is plotted against MgO. A large variability of the partial melting degree (*F%*) characterizes all the Patagonian mantle portions. In Northern Patagonia (Fig. 7a), orthopyroxene from Estancia Alvarez records an *F* of 29-30%, whereas Cerro Chenque, Puesto Diaz, and Comallo samples display an *F* between 21 and 31%. Partial melting degrees of the spinel-bearing samples from Prahuaniyeu range between 10 and 23%. On the other side, Cerro Rio Chubut, Cerro de los Chenques, and Coyhaique record *F* values up to 30% (11-30%, 14-27% and 27-30%, respectively). Central Patagonian orthopyroxenes (Fig. 7b) record the following *F* ranges: 23-26% at Chile Chico, 12-17% at Cerro Clark, 19-30% at Estancia Sol de Mayo, 22-27% at Auvernia, 8-31% at Gobernador Gregores, and 13-24% at Cerro Cuadrado and Cerro Redondo. In Southern Patagonia (Fig. 7c), the depletion event recorded by Tres Lagos orthopyroxenes are characterized by a wide *F* range (10-30%), whereas those modelled for Cerro Fraile and Las Cumbres are quite similar (13-26% and 17-25%, respectively). Finally, Pali Aike orthopyroxene records an *F* value between 12 and 18% (Table 2).

Clinopyroxene Al_2O_3 vs. MgO content and the related melt extraction models are shown in Fig. 8. In Northern Patagonia (Fig. 8a), clinopyroxene from Cerro Chenque, Puesto Piaz, Comallo, and Cerro Mojon samples record an *F* ranging between 17 and 21%. Clinopyroxene in the spinel-bearing samples of Prahuaniyeu record a highly variable *F* range, between 7 and 25%. Similar features are displayed by Cerro Rio Chubut and Cerro de los Chenques samples (*F* = 6-17% and 10-22%, respectively). Paso de los Indios clinopyroxenes record a narrower *F* range (*F* = 17-21%). According to clinopyroxene REE distributions, many of these localities (Cerro Mojon, Comallo, Prahuaniyeu, Cerro Rio Chubut, and Cerro de los Chenques) were subjected to slight to significant subsequent

enrichment processes (see below). Consequently, some of their lower *F* values (6-10%) could be affected by the action of metasomatic/refertilisation processes that may have overprinted the pristine depletion signature. In Central Patagonia (Fig. 8b), clinopyroxenes from Chile Chico, Cerro Clark, Don Camilo, Cerro Cuadrado, and Auvernia record similar melt extraction events, with *F* generally ranging between 10 and 17%. Estancia Sol de Mayo clinopyroxenes experienced greater melt extraction (*F* = 17-21%) and the highest values are comparable to those of Gobernador Gregores and Cerro Redondo, whose *F* ranges are wider (3-22% and 8-22%, respectively). The occurrence of subsequent enrichment processes was also particularly efficient in some Central Patagonian SCLM domains (Cerro Clark, Estancia Sol de Mayo and Gobernador Gregores, see below); therefore, most of the low *F* values calculated (especially those < 10%) should be considered with caution. Southern Patagonian clinopyroxenes (Fig. 8c) record large *F* intervals: between 9 and 19% at Tres Lagos, between 12 and 23% at Cerro Fraile, and between 7 and 25% in the spinel-bearing xenoliths of Pali Aike. A narrow *F* range is modelled for the La Cumbres samples, which yield a value of 17-18%. With respect to the Northern and Central regions, Southern Patagonia was less pervasively affected by subsequent enrichment processes (see below), therefore, the *F* values calculated for the latter (except those obtained for some Cerro Fraile and Pali Aike samples) could be considered more reliable than those for the former.

5.1.2. Depletion processes modelled through trace elements

Clinopyroxene trace element modelling (Fig. 9), developed by means of the PM-normalized (Sun and McDonough, 1989) Y vs. Yb diagram of Zou (1998), confirms the large variability in the partial melting degree affecting the Patagonian SCLM. In Northern Patagonia (Fig. 9a), an *F* of ~14% is obtained from Cerro Chenque clinopyroxene, whereas Puesto Diaz, Comallo, Cerro Mojon, and Prahuaniyeu samples record an *F* between 6 and 20%. Highly variable ranges are recorded by Cerro Rio Chubut and Cerro de los Chenques samples (*F* = 1-10% and 3-15%, respectively), whereas Paso de los Indios xenoliths yield almost constant values (*F* = 13-14%). Few data are available for Central

Patagonia (Fig. 9b), where clinopyroxene trace element concentration records *F* between 1 and 8% at Cerro Clark, Don Camilo and Cerro Cuadrado, whereas a higher range is obtained from the Gobernador Gregores samples (*F* = 3-17%). The melt extraction recorded by clinopyroxene is quite variable in Southern Patagonia, where *F* ranges from 1 to 14% at Tres Lagos, 4 to 21% at Cerro Fraile, 5 to 12% at Las Cumbres and 2 to 24% in Pali Aike spinel-bearing samples (Fig. 9c).

5.2. Enrichment processes

As already described in section 4.1, a widespread negative correlation between Sr_N and $(La/Yb)_N$ and Al_2O_3 is also present in many Patagonian localities such as Cerro Mojon, Prahuaniyeu, Paso de los Indios, Cerro de los Chenques, Don Camilo, Estancia sol de Mayo, and Pali Aike (Fig. 5a and 5d). This feature is consistent with the occurrence of enrichment processes able to modify the trace element composition of the clinopyroxenes after a melt extraction event (Al_2O_3 depletion). In this case, the amount of melt/fluid interacting with the previously depleted clinopyroxene was relatively small, hence leading to identify this enrichment process as "metasomatism".

However, a positive correlation between Al_2O_3 and both $(La/Yb)_N$ (Fig. 5b) and Sr_N (Fig. 5e) is displayed by some Cerro Rio Chubut and Gobernador Gregores samples, even though many of them are typified by an Al_2O_3 increase at nearly constant $(La/Yb)_N$ and Sr_N values. A positive correlation between Al_2O_3 and Sr_N also typifies samples from other Patagonian localities, and is particularly evident for Tres Lagos (Fig. 5e). Such a positive correlation between trace elements and Al_2O_3 can be interpreted in two different ways; these are functions of two opposite processes affecting the SCLM. The first is melt extraction, which would result in a decrease in both $(La/Yb)_N$ and Sr_N together with Al_2O_3. The second is a significant enrichment, which could restore the initial concentration of these trace elements simultaneously with Al_2O_3 increase. This latter process, previously defined as "refertilisation", would necessitate high melt (or fluid)/rock ratios or, alternatively, longer interaction time between the mantle domain and the percolating melt, capable of obliterating the previous depletion features and restoring a fertile composition. This is the case for

Gobernador Gregores xenoliths where significant modal amounts of amphibole and phlogopite formed during a pervasive enrichment process subsequent to a melt extraction event (up to 31% *F* according to orthopyroxene major element composition).

In some Northern, Central, and Southern Patagonia localities, neither a positive nor a negative correlation between trace elements and Al_2O_3 content of clinopyroxene was noticed. This behaviour, typical of mantle xenoliths from Estancia Alvarez, Cerro Cuadrado, and Las Cumbres (Figs. 5c and 5f), represents a third kind of SCLM evolution. After a melt extraction event that depleted clinopyroxene in both Al_2O_3 and trace elements, the circulation of variable amounts of fluids/melts re-added to the system incompatible elements and LREE. This melt-rock interaction, however, was unable to restore the Al_2O_3 content of clinopyroxene and therefore, to re-build a fertile composition and the high $(La/Yb)_N$ and Sr_N values suggest that a metasomatic event, rather than complete refertilisation, followed the partial melting.

6. Timing and distribution of the depletion and enrichment processes in the Patagonian SCLM

6.1. Mantle components

The application of mixing models (equation B.7 in Appendix B) to the Sr and Nd systematics enabled us to establish in what proportions the DMM, EM I, and EM II reservoirs contributed to generating the isotopic signature of the Patagonian SCLM (Fig. 10). A first model was developed by considering possible mixing between the DMM (Workman and Hart, 2005) and the EM I (Zindler and Hart, 1986) mantle components, adopting the same parameters used by Kay et al. (2013) for modelling the source of Patagonian plateau lavas. Afterwards, two different mixing models between DMM and an EM II component ($^{87}Sr/^{86}Sr = 0.7075$; $^{143}Nd/^{144}Nd = 0.51263$; Nd = 54.5 ppm; Hart, 1988) were advanced by varying the Sr concentration of the latter from 750 to 140 ppm (changing its Sr/Nd ratio from 13.8 to 2.6). Results showed that all Patagonian samples have scattered distributions, plotting between the DMM-EM I and the DMM-EM II mixing trends (Fig. 10) and thus further confirming a variably efficient role played by the enrichment processes in obliterating the pristine signature (Fig. 10a). The

xenoliths have Sr-Nd isotopic ratios comparable to those of the Patagonian plateau lavas ($^{87}Sr/^{86}Sr$ = 0.7031-0.7053; $^{143}Nd/^{144}Nd$ = 0.51248-0.51293), whose signature was ascribed to mixing processes between DMM and both EM I and EM II components (i.e. Gorring et al., 2003; Kay et al., 2013). According to Gorring et al. (2003), the EM II-like contribution could be ascribed to the addition of sediments and/or fluids to the Patagonian SCLM during Phanerozoic subduction processes, whereas the EM I-like component could have been generated by the infiltration of ocean island basalts (OIB)-type pulses into the mantle during Gondwana breakup and Cenozoic magmatism. By contrast, Kay et al. (2013) hypothesized that the EM I component represents the incorporation of continental lithosphere into the mantle source by lithospheric and crustal detachment, sediment subduction, and/or forearc erosion. As shown in Fig. 10a, Patagonian xenoliths plot close to both the DMM-EM I and DMM-EM II mixing curves, without showing any preferential alignment as functions of their geographical provenance and/or age of extraction (see Table 2). As observed by Gorring et al. (2003), for some post-plateau lava, it is quite difficult to determine whether the enriched component is EM I- or EM II-type. The Sr-Nd isotopic signature of most of the Northern, Central, and Southern Patagonia xenoliths could be explained by mixing between 94-99% DMM and 1-5% EM II (at 140 ppm Sr), or, alternatively, between >99% DMM and <1% EM-I components. It should be noted that a good alignment is observed for websteritic/wehrlitic samples, irrespective of their geographical provenance (Fig. 10b). In contrast with the widespread dispersion of lherzolites and harzburgites, websterites and wehrlites plot along the mixing trend between DMM and EM II (at 140 ppm Sr), suggesting that the involvement of 1-5% of an EM II component is more likely to explain their genesis (Fig. 10b).

6.2. Timing of melt extraction from Northern to Southern Patagonia

Notwithstanding the similar Sr-Nd isotopic signature and the highly variable composition, Patagonia mantle xenoliths show systematic geochemical features and provide precise information about the distribution of depletion/enrichment processes in the SCLM wedge. On the basis of bulk rock Re-Os systematics, several authors proposed a strongly heterogeneous nature for the SCLM beneath

Patagonia (Mundl et al., 2015, 2016; Schilling et al., 2008, 2017). According to these authors, the lithosphere beneath Patagonia is composed of several portions that experienced variable depletion events at different times since the Palaeoproterozoic (<2.5 Ga). Their original depletion signature was at least partially obscured by subsequent enrichment processes, among which those related to the Mesozoic to present-day Andean subduction and the Cenozoic magmatism are certainly the best preserved and identifiable.

If we compare the averaged partial melting degree recorded by orthopyroxene major elements (Al_2O_3 and MgO) with the latitude of the various localities (Fig. 11a), a decrease in *F* from ca. 30% in Northern Patagonia to ca. 15% in the Southern regions is observed. A comparable trend is displayed by clinopyroxene (from *F* ca. 25% in Northern Patagonia to ca. 16% in Southern Patagonia; Fig. 11b). Average partial melting degrees recorded by clinopyroxene trace elements are slightly lower than those obtained by major elements modelling, ranging from ca. 15% in the Northern localities to ca. 7-12% in the Central/Southern ones (Fig. 11c). Consistently, the average Fo content of olivine decreases from 90.0-91.6 in Northern Patagonia to 89.1-90.7 in Southern Patagonia (Fig. 11d). Since the Northern Patagonia xenoliths recording the highest melt extraction degrees are brought to the surface by the most recent magmatic episodes (1-5 Ma; Fig. 11f; Table 2), we cannot exclude that they could represent fragments of the SCLM bearing witness to the previous melting event, linked to tholeiite production during the main plateau phase at Somoncura (i.e. ~20% *F*; Kay et al., 2007).

A positive correlation can be also found between latitude and the average T_{RD} (Re-Os) age obtained for each Patagonian locality (Mundl et al., 2015, 2016; Schilling et al., 2008, 2017; Fig. 11e), suggesting that the Southern Patagonia SCLM domains experienced minor melt extractions in older times with respect to the Northern Patagonia region. No correlation between latitude and Sr-Nd isotopic signature of the mantle xenoliths can be envisaged, probably because of the obliterating action of the recent enrichment processes. Analogously, the trace element (REE and Sr) and Al_2O_3 contents in clinopyroxene show no link with latitude, as evidenced by the variable occurrence of both positive and negative correlations in the Northern, Central, and Southern Patagonia localities (Fig. 5).

6.3. Nature and timing of the enrichment processes

In this section, the major/trace element composition of clinopyroxenes from Northern, Central and Southern Patagonia wehrlites, websterites, orthopyroxenites and clinopyroxenites (Fig. 12) is considered to speculate about the enrichment processes and their distribution in the Northern, Central and Southern Patagonia SCLM domains. Clinopyroxenes from Northern Patagonia websterites can be subdivided into two distinct groups. The first one is characterized by high Al_2O_3/Mg# ratio (Fig. 12a) and LREE-depleted patterns (Fig. 12b) and is composed of Cerro de los Chenques websterites. The second one has lower Al_2O_3/Mg# ratios (Fig. 12a), relatively depleted heavy rare earth elements (HREE) and flat to slightly LREE-enriched patterns and comprises Cerro Aznares, Prahuaniyeu and Cerro Rio Chubut websterites (Fig. 12c). Clinopyroxenes in the few Central Patagonia websterites (Cerro Clark and Gobernador Gregores) lie on the high Al_2O_3/Mg# trend (Fig. 12a). Their REE patterns vary from slightly LREE-depleted (thus comparable to clinopyroxene in Northern Patagonia websterites, Fig. 12d) to strongly LREE-enriched (only one sample from Gobernador Gregores, Fig. 12e). Clinopyroxenes in Central Patagonia clinopyroxenites and wehrlites (Cerro Clark, Estancia Sol de Mayo and Gobernador Gregores) belong to both the high Al_2O_3/Mg# and the low Al_2O_3/Mg# groups (Fig. 12a). The REE patterns of Cerro Clark clinopyroxenites are generally depleted and similar to those of the corresponding websterites (Fig. 12d). Clinopyroxenes from Estancia Sol de Mayo and Gobernador Gregores wehrlites, however, have the most LREE-enriched and convex-upward patterns (Fig. 12e). Clinopyroxenes from Southern Patagonia clinopyroxenites (Cerro Fraile) generally fall in a narrow Al_2O_3-Mg# interval (Fig. 12a) and have flat REE profiles (Fig. 12f). Clinopyroxenes from Southern Patagonia orthopyroxenites (Cerro Fraile) plot on the low Al_2O_3/Mg# trend (Fig. 12a) and are slightly LREE-enriched, with respect to the corresponding clinopyroxenites, at comparable HREE contents (Fig. 12g).

According to Dantas (2007) and Melchiorre et al. (2015), the LREE-depleted pattern of clinopyroxenes from Northern Patagonia websterites belonging to the high Al_2O_3/Mg# group provide

the evidence for percolation of tholeiitic-like melt in the Patagonian SCLM. Consistently, clinopyroxenes from lherzolites/harzburgites are aligned on the high Al_2O_3/Mg# enrichment trend (Fig. 2), further suggesting that a tholeiitic-like melt infiltrated the mantle domains. These findings are consistent with those of D'Orazio et al. (2000), Gorring et al. (2003), and Kay et al. (2007; 2013), who recognized the existence of a tholeiitic main plateau stage in the Somoncura region. In contrast, the LREE-enriched patterns of clinopyroxenes with lower Al_2O_3/Mg# ratios are ascribable to the percolation of a CaO-rich and SiO_2-undersaturated, transitional to alkaline melt in the SCLM. The alkaline-like enrichment was not efficient enough to eradicate the pristine depletion event in terms of major elements. The alkaline event was preserved only as some LREE-enriched patterns of refractory clinopyroxenes (harzburgites and lherzolites at Cerro Mojon, Comallo, Prahuaniyeu, Cerro Rio Chubut, and Cerro de los Chenques). The occurrence of alkaline melts has been widely documented throughout this region, especially during the post-plateau magmatic stages (D'Orazio et al., 2000; Kay et al., 2007; 2013).

The bimodal occurrence of tholeiitic and alkaline enrichment processes is also evidenced beneath Central Patagonia, where clinopyroxene from lherzolites/harzburgites plot along both the high and low Al_2O_3/Mg# trends (Fig. 2). This is also suggested by the occurrence of LREE-depleted clinopyroxenes with high Al_2O_3/Mg# in Cerro Clark websterites and LREE-enriched clinopyroxenes with low Al_2O_3/Mg# in Estancia Sol de Mayo and Gobernador Gregores wehrlites. However, some clinopyroxenes from Estancia Sol de Mayo and Gobernador Gregores wehrlites have "intermediate" geochemical features, with high Al_2O_3/Mg# ratios but LREE-enriched profiles. These features are possibly consistent with the infiltration of transitional affinity melts in the SCLM. As already highlighted by Melchiorre et al. (2015), a transitional-type agent percolating through the mantle is capable of moving above and below the saturation threshold, as a function of orthopyroxene reaction/dissolution or crystallization at the expense of olivine or as a newly forming phase (Arai et al., 2006).

Broadly speaking, $(La/Yb)_N$ and Sr_N enrichment - concomitant with Al_2O_3 depletion of clinopyroxene - are evidence of a metasomatic process (lower melt/rock ratio) and recorded in many localities of Northern and Central Patagonia. A refertilisation event (simultaneous trace element and Al_2O_3 enrichment) occurred instead in the SCLM portions beneath Cerro Rio Chubut and Gobernador Gregores, where large amounts of hydrous melt interacted with the previously depleted mantle, leading to the formation of significant modal amphibole and phlogopite. In this framework, the rare presence of websteritic xenoliths with both low and high Al_2O_3/Mg# and LREE-enriched clinopyroxenes in Northern/Central Patagonia could bear witness of both a (first) tholeiitic refertilisation and a (second) alkaline metasomatism, showing two subsequent processes characterized by progressively decreasing melt/rock ratios. Further evidence of the action of metasomatic and refertilisation processes could be provided by the Sr-Nd isotopic systematics. Irrespective of their geographical provenance, clinopyroxenes belonging to refertilised SCLM portions (with positive correlation between trace elements and Al_2O_3 content) are generally depleted in $^{87}Sr/^{86}Sr$ with respect to those belonging to the metasomatized suites, suggesting an interaction with melts derived from a source with higher asthenospheric contribution (Fig. 10c). Altogether, these data suggest that the SCLM portions beneath Cerro Rio Chubut (Northern Patagonia) and Gobernador Gregores (Central Patagonia) may have experienced both tholeiitic refertilisation and alkaline metasomatism.

In Southern Patagonian lherzolites/harzburgites, no evidence of tholeiitic and/or alkaline enrichment is generally provided by the major/trace element distribution of clinopyroxene, which lies at narrow Al_2O_3 and Mg# intervals (Fig. 2), thus confirming that melt extraction was the main process acting in the SCLM (Ntaflos et al., 2007). Similar behaviour characterizes clinopyroxene from clinopyroxenites (Fig. 12a). An exception is constituted by a few Pali Aike samples, where the moderate LREE-enrichment of clinopyroxene probably occurred due to the interaction with alkaline agents. A spatially limited involvement of SiO_2-saturated melts is instead suggested by Cerro Fraile

orthopyroxenites, whose formation was ascribed to the percolation of proto-adakitic agents into the mantle wedge sectors closer to the trench (Faccini et al., 2013).

7. Conclusions

In this work, a review of the main geochemical features of all Patagonian mantle xenoliths, together with new Sr-Nd isotopic data on clinopyroxene separates from representative suites enabled us to establish some significant points:

1. Two common Al_2O_3/Mg# trends characterize clinopyroxenes and orthopyroxenes from Patagonia mantle xenoliths, and a systematic distribution can be identified in clinopyroxenes and orthopyroxenes in harzburgites/lherzolites are isolated from those belonging to wehrlites, websterites, dunites, orthopyroxenites, and clinopyroxenites. Northern Patagonia clinopyroxenes lie on a well-defined high Al_2O_3/Mg# trend; the distribution of those from Central Patagonia xenoliths is scattered and follows both a high Al_2O_3/Mg# and a low Al_2O_3/Mg# trend; a narrower compositional spectrum typified Southern Patagonia clinopyroxenes.

2. Trace element content of clinopyroxenes suggests that the SCLM beneath Patagonia is extremely heterogeneous. At Cerro Rio Chubut and Gobernador Gregores, the positive correlations between $(La/Yb)_N$ and Sr_N and Al_2O_3, together with the modal occurrence of amphibole and phlogopite, favour the involvement of long-lasting enrichment processes, or, alternatively, of high melt(fluid)/rock ratios, capable of restoring fertile conditions in the mantle (refertilisation). The negative correlations between $(La/Yb)_N$ and Sr_N and Al_2O_3 and/or the absence of a well-defined trend in most Patagonian localities are consistent with a variable action of enriched fluids/melts pervading the SCLM. Such processes, which occurred in a relatively limited timespan or were characterized by lower melt(fluid)/rock ratios, can be defined as metasomatism. A few portions of the mantle are instead devoid of significant metasomatic features, as suggested by Ntaflos et al. (2007).

3. The partial melting degree recorded by clinopyroxenes and orthopyroxenes in Patagonian harzburgites and lherzolites ranges from 1% to 30%. Results from partial melting models show that

a progressively decreasing partial melting degree is recorded moving from Northern to Southern Patagonia. Consistently, forsterite content of olivine decreases from Northern to Southern Patagonia samples. The calculated *F* values for Northern Patagonia xenoliths are also consistent with the partial melting degrees proposed in the literature to explain the generation of the Somoncura lavas (Kay et al., 2007). Coupled with the Re-Os age data recently proposed by Mundl et al. (2015, 2016) and Schilling et al. (2008, 2017), these features suggest that the SCLM domains beneath Southern Patagonia experienced lower melt extractions in older times with respect to the Northern ones.

4. The overlap between the Sr-Nd isotopic signature of Northern, Central, and Southern Patagonia clinopyroxenes is ascribable to the "obliterating" action of recent enrichment processes, as also testified by the overlap in the distribution of the plateau lavas (Gorring et al., 2003; Kay et al., 2013). Some mantle xenoliths align quite well along the mixing curve between DMM and EM II, even if the scattered data distribution makes it difficult to discriminate between the EM I and EM II contributions. Irrespective of the geographical provenance, extraction age, and distance between sampling localities of the xenoliths and the trench, clinopyroxenes from websterites and wehrlites plot along the mixing trend between a DMM and EM II component. Altogether, these data suggest that both the addition of sediments fluids during subduction-related processes and the occurrence of OIB-like pulses during Cenozoic plateau magmatism could have overprinted the Sr-Nd signature of Patagonian mantle xenoliths.

5. Northern Patagonia SCLM was infiltrated by tholeiitic melts that modified the major/trace element composition of clinopyroxene in harzburgites/lherzolites and generated high Al_2O_3/Mg# and LREE-depleted patterns of clinopyroxene in websterites. Evidence of the existence of tholeiitic enrichment is provided by the REE-depleted patterns of clinopyroxene inside harzburgites/lherzolites from some localities (Estancia Alvarez, Cerro Chenque, Puesto Diaz, Paso de los Indios). The presence of a poorly efficient alkaline enrichment process is instead recorded by some LREE-enriched high Mg# clinopyroxenes in harzburgites/lherzolites (Cerro Mojon, Comallo, Prahuaniyeu, Cerro Rio Chubut, and Cerro de los Chenques), as well as by websteritic xenoliths with low Al_2O_3/Mg# and LREE-

enriched clinopyroxenes. In Central Patagonia, both a tholeiitic and an alkaline enrichment process modified the major/trace element composition of clinopyroxene in lherzolites/harzburgites and generated websteritic and wehrlitic domains. The interaction with a tholeiitic melt is demonstrated at Cerro Clark, where both websterites and harzburgites/lherzolites with LREE-depleted clinopyroxenes were documented. However, the percolation of an alkaline agent is hypothesized for Estancia Sol de Mayo and Gobernador Gregores, where wehrlites and harzburgites/lherzolites with LREE-enriched clinopyroxenes were found. The "intermediate" behaviour of some clinopyroxenes in websterites and wehrlites (high Al_2O_3/Mg# but LREE-enriched patterns) are consistent with the involvement of a melt with transitional affinity beneath Estancia Sol de Mayo and Gobernador Gregores. Melt extraction is the main process recorded by Southern Patagonian xenoliths (Ntaflos et al., 2007), even if the geochemical features of some clinopyroxenes from Pali Aike and Cerro Fraile harzburgites/lherzolites lead to speculation that these two SCLM domains interacted with alkaline and SiO_2-saturated proto-adakitic agents, respectively (Dantas, 2007; Faccini et al., 2013; Mundl et al., 2015).

6. The occurrence of both tholeiitic and alkaline enrichments in the Patagonia SCLM is consistent with the evolutionary sequence described by D'Orazio et al. (2004), Gorring et al. (2003) and Kay et al. (2007; 2013) for Patagonian plateau magmatism, where limited alkaline pulses followed the emission of large volumes of tholeiitic lavas. In this framework, it is likely to imagine that a first tholeiitic enrichment process beneath Northern-Central Patagonia SCLM was followed by the percolation of transitional-alkaline agents, even if the infiltration of subduction-derived melts/fluids into the mantle wedge cannot be excluded and is still debated (Gorring et al., 2003; Kay et al., 2013).

7. A systematic Sr-Nd discrimination between clinopyroxenes in refertilised mantle suites (Cerro Rio Chubut and Gobernador Gregores) and those belonging to metasomatized ones can be done. The general Sr isotopic depletion of the formers highlights that the refertilisation processes in the Patagonian SCLM were caused by long-lasting reactions between the depleted mantle and the transitional-alkaline enrichment agents.

Acknowledgements

This work is part of a co-tutorship Ph.D. held within the 2008 Vinci Project "Matter transfer in suprasubductive mantle in complex converging systems". The project was funded by the Italian National Research Program [PRIN_2017 Project 20178LPCPW] to [MC], and by the "Università Italo-Francese". The activities were conducted between the University of Ferrara and the Observatoire Midi-Pyrenees in Toulouse. MM appreciates the support of the project ALPIMED (PIE-CSIC-201530E082). We thank the laboratory staff of the UMR 5563 (GET, Observatoire Midi-Pyrenees) of the University Paul Sabatier (Toulouse III) for their support during the performance of TIMS analyses.

References

Aliani, P., Ntaflos, T., Bjerg, E., 2009. Origin of melt pockets in mantle xenoliths from southern Patagonia, Argentina. Journal of South American Earth Sciences 28, 419-428.

Arai, S., Shimizu, Y., Morishita, T., Ishida, Y., 2006. A new type of orthopyroxenite xenolith from Takashima, Southwest Japan: silica enrichment of the mantle by evolved alkali basalt. Contributions to Mineralogy and Petrology 152(3), 387.

Ardolino, A., Franchi, M., Remesal, M., Salani, F., 1999. El volcanismo en la Patagonia Extraandina. Geología Argentina 29, 579-612.

Benoit, M., Ceuleneer, G., Polvé, M., 1999. The remelting of hydrothermally altered peridotite at mid-ocean ridges by intruding mantle diapirs. Nature 402, 514-518.

Bjerg, E.A., Ntaflos, T., Kurat, G., Dobosi, G., Labudía, C.H., 2005. The upper mantle beneath Patagonia, Argentina, documented by xenoliths from alkali basalts. Journal of South American Earth Sciences 18, 125-145.

Bjerg, E.A., Ntaflos, T., Thöni, M., Aliani, P., Labudia, C.H., 2009. Heterogeneous lithospheric mantle beneath Northern Patagonia: Evidence from Prahuaniyeu garnet- and spinel-peridotites. Journal of Petrology 50, 1267-1298.

Bonadiman, C., Coltorti, M., 2011. Numerical modelling for peridotite phase melting trends in the SiO_2-Al_2O_3-FeO-MgO-CaO system at 2 GPa. Mineralogical Magazine 75, 548-548.

Cande, S.C., Leslie, R.B., 1986. Late Cenozoic tectonics of the southern Chile Trench. Journal of Geophysical Research 91, 471-496.

Conceição, R.V., Mallmann, G., Koester, E., Schilling, M., Bertotto, G.W., Rodriguez-Vargas, A., 2005. Andean subduction-related mantle xenoliths: Isotopic evidence of Sr-Nd decoupling during metasomatism. Lithos 82, 273-287.

Corbella, H., Chelotti, L., Pomposiello, C., 1996. Neotectonica del rift Jurasico austral en Pali Aike, Patagonia Extrandina, Santa Cruz, Argentina. XIII Congreso Geologico Argentino y III Congreso de Exploracion de Hidrocarburos, Actas 2, 383-393.

Dantas, C., 2007. Caractérisation du manteau supérieur Patagonien: Les enclaves ultramafiques et mafiques dans les laves alcalines. Université de Toulouse III p. 323.

Dantas, C., Grégoire, M., Koester, E., Conceição, R.V., Rieck Jr, N., 2009. The lherzolite-websterite xenolith suite from Northern Patagonia (Argentina): Evidence of mantle-melt reaction processes. Lithos 107, 107-120.

DePaolo, D.J., Wasserburg, G.J., 1979. Petrogenetic mixing models and Nd-Sr isotopic patterns. Geochimica et Cosmochimica Acta 43, 615-627.

Diraison, M., Cobbold, P.R., Gapais, D., Rossello, E.A., 1997. Magellan Strait: Part of a Neogene rift system. Geology 25, 703-706.

D'Orazio, M., Agostini, S., Mazzarini, F., Innocenti, F., Manetti, P., Haller, M.J., Lahsen, A., 2000. The Pali Aike Volcanic Field, Patagonia: Slab-window magmatism near the tip of South America. Tectonophysics 321, 407-427.

D'Orazio, M., Innocenti, F., Manetti, P., Haller, M. J., 2004. The Cenozoic back-arc magmatism of the southern extra-Andean Patagonia (44.5-52° S): A review of geochemical data and geodynamic interpretations. Revista de la Asociación Geológica Argentina 59(4), 525-538

Faccini, B., Bonadiman, C., Coltorti, M., Grégoire, M., Siena, F., 2013. Oceanic material recycled within the sub-patagonian lithospheric mantle (Cerro del Fraile, Argentina). Journal of Petrology 54, 1211-1258.

Faure, G., 1986. Principles of isotope geology. John Wiley and Sons, Inc.,New York, NY; None.

Folguera, A., Encinas, A., Echaurren, A., Gianni, G., Orts, D., Valencia, V., Carrasco, G., 2018. Constraints on the Neogene growth of the central Patagonian Andes at the latitude of the Chile triple junction (45-47° S) using U/Pb geochronology in synorogenic strata. Tectonophysics 744, 134-154.

Gorring, M.L., Kay, S.M., 2000. Carbonatite metasomatized peridotite xenoliths from southern Patagonia: Implications for lithospheric processes and Neogene plateau magmatism. Contributions to Mineralogy and Petrology 140, 55-72.

Gorring, M.L., Kay, S.M., Zeitler, P.K., Ramos, V.A., Rubiolo, D., Fernandez, M.I., Panza, J.L., 1997. Neogene Patagonian plateau lavas: Continental magmas associated with ridge collision at the Chile Triple Junction. Tectonics 16, 1-17.

Gorring, M.L., Singer, B., Gowers, J., Kay, S.M., 2003. Plio-Pleistocene basalts from the Meseta del Lago Buenos Aires, Argentina: Evidence for asthenosphere-lithosphere interactions during slab window magmatism. Chemical Geology 193, 215-235.

Hart, S.R., 1988. Heterogeneous mantle domains: signatures, genesis and mixing chronologies. Earth and Planetary Science Letters 90(3), 273-296.

Kay, S.M., Ardolino, A.A., Gorring, M.L., Ramos, V.A., 2007. The Somuncura large igneous province in Patagonia: Interaction of a transient mantle thermal anomaly with a subducting slab. Journal of Petrology 48, 43-77.

Kay, S.M., Gorring, M., Ramos, V.A., 2004. Magmatic sources, setting and causes of Eocene to recent Patagonian plateau magmatism (36°S to 52°S latitude). Revista de la Asociacion Geologica Argentina 59, 556-568.

Kay, S.M., Jones, H.A., Kay, R.W., 2013. Origin of Tertiary to Recent EM-and subduction-like chemical and isotopic signatures in Auca Mahuida region (37–38 S) and other Patagonian plateau lavas. Contributions to Mineralogy and Petrology 166(1), 165-192.

Kay, S.M., Ramos, V.A., Mpodozis, C., Sruoga, P., 1989. Late Paleozoic to Jurassic silicic magmatism at the Gondwana margin: analogy to the Middle Proterozoic in North America? Geology 17, 324-328.

Kilian, R., Stern, C.R., 2002. Constraints on the interaction between slab melts and the mantle wedge from adakitic glass in peridotite xenoliths. European Journal of Mineralogy 14, 25-36.

Laurora, A., Mazzucchelli, M., Rivalenti, G., Vannucci, R., Zanetti, A., Barbieri, M.A., Cingolani, C.A., 2001. Metasomatism and melting in carbonated peridotite xenoliths from the mantle wedge: The Gobernador Gregores case (Southern Patagonia). Journal of Petrology 42, 69-87.

Le Roux, V., Bodinier, J.L., Tommasi, A., Alard, O., Dautria, J.M., Vauchez, A., Riches, A.J.V., 2007. The Lherz spinel lherzolite: Refertilized rather than pristine mantle. Earth and Planetary Science Letters 259, 599-612.

MacGregor, I.D., 1974. The system MgO-Al2O3-SiO2: Solubility of Al2O3 in enstatite for spinel and garnet peridotite compositions. Am. Mineral. 59, 110-119.

McDonough, W.F., Sun, S.S., 1995. The composition of the Earth. Chemical Geology 120, 223-253.

Melchiorre, M., Coltorti, M., Gregoire, M., Benoit, M., 2015. Refertilization process in the Patagonian subcontinental lithospheric mantle of Estancia Sol de Mayo (Argentina). Tectonophysics 650, 124-143.

Mercier, J.C.C., Nicolas, A., 1975. Textures and fabrics of upper-mantle peridotites as illustrated by xenoliths from basalts. Journal of Petrology 16, 454-487.

Mundl, A., Ntaflos, T., Ackerman, L., Bizimis, M., Bjerg, E.A., Hauzenberger, C.A., 2015. Mesoproterozoic and Paleoproterozoic subcontinental lithospheric mantle domains beneath southern Patagonia: Isotopic evidence for its connection to Africa and Antarctica. Geology 43(1), 39-42.

Mundl, A., Ntaflos, T., Ackerman, L., Bizimis, M., Bjerg, E.A., Wegner, W., Hauzenberger, C.A., 2016. Geochemical and Os–Hf–Nd–Sr Isotopic Characterization of North Patagonian Mantle Xenoliths: Implications for Extensive Melt Extraction and Percolation Processes. Journal of Petrology 57(4), 685-715.

Ntaflos, T., Bjerg, E.A., Labudia, C.H., Kurat, G., 2007. Depleted lithosphere from the mantle wedge beneath Tres Lagos, southern Patagonia, Argentina. Lithos 94, 46-65.

O'Reilly, S.Y., Griffin W.L., 2013. Mantle Metasomatism. In: Metasomatism and the Chemical Transformation of Rock. Lecture Notes in Earth System Sciences. Springer, Berlin, Heidelberg.

Pankhurst, R.J., Rapela, C.R., 1995. Production of Jurassic rhyolite by anatexis of the lower crust of Patagonia. Earth and Planetary Science Letters 134, 23-36.

Pelorosso, B., Bonadiman, C., Coltorti, M., Faccini, B., Melchiorre, M., Ntaflos, T., Gregoire, M., 2016. Pervasive, tholeiitic refertilisation and heterogeneous metasomatism in Northern Victoria Land lithospheric mantle (Antarctica). Lithos 248-251, 493-505.

Ramos, V.A., Kay, S.M., 1992. Southern Patagonian plateau basalts and deformation: Backarc testimony of ridge collisions. Tectonophysics 205, 261-282.

Ramos, V.A., Riccardi, A.C., Rolleri, E.O., 2004. Límites naturales del norte de la Patagonia. Revista de la Asociación Geológica Argentina 59(4), 785-786.

Rapela, C.W., Kay, S.M., 1988. Late Paleozoic to recent magmatic evolution of northern Patagonia. Episodes 11, 175-182.

Rapela, C.W., Spalletti, L.A., Merodio, J.C., Aragón, E., 1988. Temporal evolution and spatial variation of early tertiary volcanism in the Patagonian Andes (40°S-42°30′S). Journal of South American Earth Sciences 1, 75-88.

Rivalenti, G., Mazzucchelli, M., Laurora, A., Ciuffi, S.I.A., Zanetti, A., Vannucci, R., Cingolani, C.A., 2004. The backarc mantle lithosphere in Patagonia, South America. Journal of South American Earth Sciences 17, 121-152.

Rivalenti, G., Mazzucchelli, M., Zanetti, A., Vannucci, R., Bollinger, C., Hémond, C., Bertotto, G.W., 2007. Xenoliths from Cerro de los Chenques (Patagonia): An example of slab-related metasomatism in the backarc lithospheric mantle. Lithos 99, 45-67.

Schilling, M.E., Carlson, R.W., Conceição, R.V., Dantas, C., Bertotto, G.W., Koester, E., 2008. Re-Os isotope constraints on subcontinental lithospheric mantle evolution of southern South America. Earth and Planetary Science Letters 268(1-2), 89-101.

Schilling, M.E., Carlson, R.W., Tassara, A., Conceição, R.V., Bertotto, G.W., Vásquez, M., ..., Morata, D., 2017. The origin of Patagonia revealed by Re-Os systematics of mantle xenoliths. Precambrian Research 294, 15-32.

Schilling, M.E., Conceição, R.V., Mallmann, G., Koester, E., Kawashita, K., Hervé, F., ..., Motoki, A., 2005. Spinel-facies mantle xenoliths from Cerro Redondo, Argentine Patagonia: Petrographic, geochemical, and isotopic evidence of interaction between xenoliths and host basalt. Lithos 82(3-4), 485-502.

Scott, J. M., Liu, J., Pearson, D.G., Waight, T.E., 2016. Mantle depletion and metasomatism recorded in orthopyroxene in highly depleted peridotites. Chemical Geology 441, 280-291.

Snow, J.E., Hart, S.R., Dick, H.J.B., 1994. Nd and Sr isotope evidence linking mid-ocean-ridge basalts and abyssal peridotites. Nature 371, 57-60.

Stern, C.R., Kilian, R., 1996. Role of the subducted slab, mantle wedge and continental crust in the generation of adakites from the Andean Austral Volcanic Zone. Contributions to Mineralogy and Petrology 123, 263-281.

Stern, C.R., Kilian, R., Olker, B., Hauri, E.H., Kyser, T.K., 1999. Evidence from mantle xenoliths for relatively thin (< 100 km) continental lithosphere below the Phanerozoic crust of southernmost South America. In Developments in Geotectonics. Elsevier, vol. 24, pp. 217-235.

Stern, C.R., Saul, S., Skewes, M.A., Futa, K., 1989. Garnet peridotite xenoliths from the Pali-Aike alkali basalts of southernmost South America. Kimberlites and Related Rocks 14, 735-744.

Sun, S.S., McDonough, W.F., 1989. Chemical and isotopic systematics of oceanic basalts: implications for mantle composition and processes. Magmatism in the ocean basins, 313-345.

Thomson, S.N., Brandon, M.T., Tomkin, J.H., Reiners, P.W., Vasquez, C., Wilson, N.J., 2010. Glaciation as a destructive and constructive control on mountain building. Nature 467, 313-317.

Upton, B.G.J., Downes, H., Kirstein, L.A., Bonadiman, C., Hill, P.G., Ntaflos, T., 2011. The lithospheric mantle and lower crust-mantle relationships under Scotland: A xenolithic perspective. Journal of the Geological Society 168, 873-886.

Walter, M.J., 2003. Melt extraction and compositional variability in mantle lithosphere. The Mantle & Core. Treatise of Geochemistry 2, 363-394.

Workman, R.K., Hart, S.R., 2005. Major and trace element composition of the depleted MORB mantle (DMM). Earth and Planetary Science Letters 231, 53-72.

Zindler, A., Hart, S., 1986. Chemical geodynamics. Annual review of Earth and planetary sciences. Vol. 14, 493-571.

Zou, H., 1998. Trace element fractionation during modal and nonmodal dynamic melting and open-system melting: a mathematical treatment. Geochimica et Cosmochimica Acta 62, 1937-1945.

Figure captions

Fig. 1 (colour online)

Topographic and tectonic map of Patagonia showing the distribution of the Eocene to present days back arc plateau lavas and the known mantle xenoliths-bearing localities (modified after Kay et al., 2007; Thomson et al., 2010). Dashed lines identify Northern (39/40-46° S), Central (46-49° S) and Southern Patagonia (49-52° S). Northern Patagonia: 1 = Laguna Fria; 2 = Cerro Chenque; 3 = Puesto Diaz; 4 = Estancia Alvarez; 5 = Cerro Aznares; 6 = Comallo; 7 = Cerro Mojon; 8 = Prahuaniyeu; 9 = Traful; 10 = Cerro Rio Chubut; 11 = Paso de los Indios; 12 = Cerro de los Chenques; 13 = Coyhaique. Central Patagonia: 14 = Chile Chico; 15 = Cerro Clark; 16 = Estancia Sol de Mayo; 17 = Don Camilo; 18 = Cerro Cuadrado; 19 = Auvernia; 20 = Gobernador Gregores (+ Estancia Lote 17); 21 = Cerro Redondo. Southern Patagonia: 22 = Tres Lagos; 23 = Cerro Fraile; 24 = Las Cumbres; 25 = Pali Aike (data from Aliani et al., 2009; Bjerg et al., 2005, 2009; Conceicao et al., 2005; Dantas, 2007; Dantas et al., 2009; Faccini et al., 2013; Gorring and Kay, 2000; Kilian and Stern, 2002; Laurora et al., 2001; Melchiorre et al., 2015; Mundl et al., 2015, 2016; Ntaflos et al., 2007; Rivalenti et al., 2004, 2007; Schilling et al., 2005, 2008, 2017; Stern et al., 1999).

Fig. 2 (colour online)

Al_2O_3 (wt%) vs. Mg# diagrams showing the distribution of clinopyroxenes in Patagonian mantle xenoliths (from Aliani et al., 2009; Bjerg et al., 2005, 2009; Conceicao et al., 2005; Dantas, 2007; Dantas et al., 2009; Faccini et al., 2013; Gorring and Kay, 2000; Kilian and Stern, 2002; Laurora et al., 2001; Melchiorre et al., 2015; Mundl et al., 2015, 2016; Ntaflos et al., 2007; Rivalenti et al., 2004, 2007; Schilling et al., 2005, 2008, 2017; Stern et al., 1999). In the upper panels is reported the composition of clinopyroxene in harzburgites and lherzolites from (a) Northern, (b) Central, and (c) Southern Patagonia. In the lower panels is reported the composition of clinopyroxene in dunites, wehrlites, websterites, orthopyroxenites and clinopyroxenites from (d) Northern, (e) Central, and (f) Southern Patagonia.

Fig. 3 (colour online)

Al_2O_3 (wt%) vs. Mg# diagrams showing the distribution of orthopyroxenes in Patagonian mantle xenoliths (from Aliani et al., 2009; Bjerg et al., 2005, 2009; Conceicao et al., 2005; Dantas, 2007; Dantas et al., 2009; Faccini et al., 2013; Gorring and Kay, 2000; Kilian and Stern, 2002; Laurora et al., 2001; Melchiorre et al., 2015; Mundl et al., 2015, 2016; Ntaflos et al., 2007; Rivalenti et al., 2004, 2007; Schilling et al., 2005, 2008, 2017; Stern et al., 1999). In the upper panels the composition of orthopyroxene in harzburgites and lherzolites from (a) Northern, (b) Central, and (c) Southern Patagonia is reported. In the lower panels the composition of orthopyroxene in dunites, wehrlites, websterites, orthopyroxenites, and clinopyroxenites from (d) Northern, (e) Central, and (f) Southern Patagonia is reported.

Fig. 4 (colour online)

NiO (wt%) vs. Fo diagrams showing the composition of olivine in harzburgitic and lherzolitic (circles) and in dunitic, wehrlitic, websteritic, and orthopyroxenitic (crosses) xenoliths from (a) Northern, (b) Central, and (c) Southern Patagonia. Data from Aliani et al. (2009), Bjerg et al. (2005, 2009), Conceicao et al. (2005),; Dantas (2007), Dantas et al. (2009), Faccini et al. (2013), Gorring and Kay (2000), Kilian and Stern (2002), Laurora et al. (2001), Melchiorre et al. (2015), Mundl et al. (2015, 2016), Ntaflos et al. (2007) Rivalenti et al. (2004, 2007), Schilling et al. (2005, 2008, 2017), and Stern et al. (1999).

Fig. 5 (colour online)

Chondrite-normalized (Sun and McDonough, 1989) La/Yb (a, b, c) and Sr (d, e, f) vs. Al_2O_3 (wt%) diagrams showing the behavior of clinopyroxenes from Northern, Central, and Southern Patagonia mantle xenoliths. (a) Clinopyroxenes characterized by negative correlation between $(La/Yb)_N$ and Al_2O_3 (wt%); (b) clinopyroxenes with positive correlation between $(La/Yb)_N$ and Al_2O_3 (wt%); (c) clinopyroxenes without any clear correlation between $(La/Yb)_N$ and Al_2O_3 (wt%); (d) clinopyroxene showing a negative correlation between Sr_N and Al_2O_3 (wt%); (e) clinopyroxenes with positive

correlation between Sr_N and Al_2O_3 (wt%); (f) clinopyroxenes without any clear correlation between Sr_N and Al_2O_3 (wt%). Data from Aliani et al. (2009), Bjerg et al. (2005, 2009), Conceicao et al. (2005),; Dantas (2007), Dantas et al. (2009), Faccini et al. (2013), Gorring and Kay (2000), Kilian and Stern (2002), Laurora et al. (2001), Melchiorre et al. (2015), Mundl et al. (2015, 2016), Ntaflos et al. (2007), Rivalenti et al. (2004, 2007), Schilling et al. (2005, 2008, 2017), and Stern et al. (1999).

Fig. 6 (colour online)

$^{143}Nd/^{144}Nd$ vs. $^{87}Sr/^{86}Sr$ diagram showing the isotopic signature of clinopyroxene separates from Cerro Rio Chubut, Cerro de los Chenques, Cerro Clark, Estancia Sol de Mayo, Gobernador Gregores, Cerro Fraile, and Pali Aike mantle xenoliths. Literature data showing the composition of clinopyroxene separates from Northern, Central, and Southern Patagonia mantle xenoliths are reported in the fields defined by the dotted, dashed-dotted and solid lines, respectively (see text for references). Depleted (DMM) and enriched (EM I; EM II) mantle end-members are from Workman and Hart (2005), Zindler and Hart (1986), and Hart (1988). Mantle array is plotted according to DePaolo and Wasserburg (1979); BSE = Bulk Silicate Earth ($^{87}Sr/^{86}Sr$ = 0.70445; $^{143}Nd/^{144}Nd$ = 0.51264; Faure, 1986).

Fig. 7 (colour online)

Al_2O_3 (wt%) vs. MgO (wt%) diagrams showing the composition of orthopyroxenes from (a) Northern, (b) Central, and (c) Southern Patagonia harzburgites and lherzolites (from Aliani et al., 2009; Bjerg et al., 2005, 2009; Conceicao et al., 2005; Dantas, 2007; Dantas et al., 2009; Faccini et al., 2013; Gorring and Kay, 2000; Kilian and Stern, 2002; Laurora et al., 2001; Melchiorre et al., 2015; Mundl et al., 2015, 2016; Ntaflos et al., 2007; Rivalenti et al., 2004, 2007; Schilling et al., 2005, 2008, 2017; Stern et al., 1999). Curves in (a), (b), and (c) are referred to the melting model of Upton et al. (2011), developed from a starting Primitive Mantle (PM) composition (McDonough and Sun, 1995). Numbers along the curves correspond to the partial melting percentages. Since Upton et al.

(2011) model works only in the spinel stability field, for Prahuaniyeu and Pali Aike localities - where both spinel- and garnet-bearing peridotites are documented - only data from spinel-bearing peridotites were plotted.

Fig. 8 (colour online)

Al_2O_3 (wt%) vs. MgO (wt%) diagrams showing the composition of clinopyroxenes from (a) Northern, (b) Central, and (c) Southern Patagonia harzburgites and lherzolites (from Aliani et al., 2009; Bjerg et al., 2005, 2009; Conceicao et al., 2005; Dantas, 2007; Dantas et al., 2009; Faccini et al., 2013; Gorring and Kay, 2000; Kilian and Stern, 2002; Laurora et al., 2001; Melchiorre et al., 2015; Mundl et al., 2015, 2016; Ntaflos et al., 2007; Rivalenti et al., 2004, 2007; Schilling et al., 2005, 2008, 2017; Stern et al., 1999). Curves in (a), (b), and (c) are referred to the melting model of Upton et al. (2011), developed from a starting Primitive Mantle (PM) composition (McDonough and Sun, 1995). Numbers along the curves correspond to the partial melting percentages. Since Upton et al. (2011) model works only in the spinel stability field, for Prahuaniyeu and Pali Aike localities - where both spinel- and garnet-bearing peridotites are documented - only data from spinel-bearing peridotites were plotted.

Fig. 9 (colour online)

Primitive mantle- (PM) normalized Yb vs. Y diagrams showing the composition of clinopyroxenes from (a) Northern, (b) Central, and (c) Southern Patagonia harzburgites and lherzolites (from Aliani et al., 2009; Bjerg et al., 2005, 2009; Conceicao et al., 2005; Dantas, 2007; Dantas et al., 2009; Faccini et al., 2013; Gorring and Kay, 2000; Kilian and Stern, 2002; Laurora et al., 2001; Melchiorre et al., 2015; Mundl et al., 2015, 2016; Ntaflos et al., 2007; Rivalenti et al., 2004, 2007; Schilling et al., 2005, 2008, 2017; Stern et al., 1999). Curves in (a), (b), and (c) are referred to the melting model of Zou (1998), developed from a starting Primitive Mantle (PM) composition (McDonough and Sun, 1995). Numbers along the curves correspond to the partial melting percentages. Since Zou (1998) model

works only in the spinel stability field, for Prahuaniyeu and Pali Aike localities - where both spinel- and garnet-bearing peridotites are documented - only data from spinel-bearing peridotites were plotted.

Fig. 10 (colour online)

$^{143}Nd/^{144}Nd$ vs $^{87}Sr/^{86}Sr$ isotopic signature of clinopyroxenes from Patagonia mantle xenoliths plotted onto the mixing curves between depleted (DMM) and enriched (EM I-EM II) mantle reservoirs. (a) Geographical subdivision of the samples (Northern vs. Central vs. Southern Patagonia). (b) Lithological subdivision of the samples (lherzolites/harzburgites vs. websterites/wehrlites). (c) Subdivision of the samples based on the correlation between trace elements (La/Yb; Sr) and Al_2O_3 of clinopyroxene (i.e. negative vs. positive; see text for further explanation). The three curves plotted in (a), (b), and (c) represent the mixing models between DMM and EM I-EM II end-members. The mixing model between DMM and EM I components is developed in accordance with Kay et al. (2013). The two mixing models between DMM and EM II were obtained by varying the Sr content of the EM II reservoir from 750 to 140 ppm, thus changing its Sr/Nd ratio from 13.8 to 2.6. The percentages of EM I-EM II components in each of the mixing models are also reported on the corresponding curves. Depleted (DMM) and enriched (EM I; EM II) mantle end-members are from Workman and Hart (2005), Zindler and Hart (1986), and Hart (1988).

Fig. 11 (colour online)

Average partial melting degrees (F%) calculated for orthopyroxenes and clinopyroxenes, forsterite content of olivines, T_{RD} (Re-Os) age recorded by mantle xenoliths and ages of the xenoliths-bearing lavas from each Patagonian locality plotted against latitude (°S). (a) Averaged partial melting degrees recorded by orthopyroxenes major element composition (Al_2O_3 vs MgO). (b) Averaged partial melting degrees recorded by clinopyroxenes major element composition (Al_2O_3 vs MgO). (c) Averaged partial melting degrees recorded by clinopyroxenes trace element composition (Y_N vs

Yb_N). (d) Averaged Fo content of olivines in lherzolites and harzburgites. (e) Averaged Rhenium depletion ages (T_{RD}; Ga) yielded by Patagonia xenoliths. (f) Age span of the xenoliths-bearing Patagonia lavas (Ma). Dotted lines indicate the subdivision between Northern (39/40-46° S), Central (46-49° S) and Southern (49-54° S) Patagonia. See text and Table 2 for further explanation and references. Source data from Aliani et al. (2009), Bjerg et al. (2005, 2009), Conceicao et al. (2005),; Dantas (2007), Dantas et al. (2009), Faccini et al. (2013), Gorring and Kay (2000), Kilian and Stern (2002), Laurora et al. (2001), Melchiorre et al. (2015), Mundl et al. (2015, 2016), Ntaflos et al. (2007), Rivalenti et al. (2004, 2007), Schilling et al. (2005, 2008, 2017), and Stern et al. (1999).

Fig. 12 (colour online)

Major element distribution and chondrite-normalized (Sun and McDonough, 1989) REE patterns of clinopyroxenes from Patagonian websterites, wehrlites, orthopyroxenites, and clinopyroxenites. (a) Al_2O_3 vs Mg# diagram showing the composition of clinopyroxenes from Northern Patagonia websterites, Central Patagonia websterites, wehrlites, and clinopyroxenites and Southern Patagonia orthopyroxenites and clinopyroxenites. The black arrows indicate the two main trend followed by clinopyroxenes (high Al_2O_3/Mg# and low Al_2O_3/Mg#), in accordance with the subdivision proposed by Melchiorre et al. (2015). (b) Chondrite-normalized REE patterns of clinopyroxenes from Northern Patagonia high Al_2O_3/Mg# websterites; field defined by solid line is referred to clinopyroxenes composition in harzburgites and lherzolites from Estancia Alvarez, Cerro Chenque, Puesto Diaz and Paso de los Indios. (c) Chondrite-normalized REE patterns of clinopyroxenes from Northern Patagonia low Al_2O_3/Mg# websterites; field defined by dotted line is referred to clinopyroxenes composition in harzburgites and lherzolites from Cerro Mojon, Comallo, Prahuaniyeu, Cerro Rio Chubut, and Cerro de los Chenques. (d) Chondrite-normalized REE patterns of clinopyroxenes from Central Patagonia high Al_2O_3/Mg# websterites and clinopyroxenites; field defined by solid line is referred to clinopyroxene composition in harzburgites and lherzolites from Cerro Clark, Don Camilo, and Cerro Cuadrado. (e) Chondrite-normalized REE patterns of clinopyroxenes from Central

Patagonia high Al_2O_3/Mg# websterites (sample from Gobernador Gregores) and wehrlites; field defined by dotted line is referred to clinopyroxenes composition in harzburgites and lherzolites from Estancia Sol de Mayo and Gobernador Gregores (+ Estancia Lote 17). (f) Chondrite-normalized REE patterns of clinopyroxenes from Southern Patagonia orthopyroxenites. (g) Chondrite-normalized REE patterns of clinopyroxene from Southern Patagonia clinopyroxenites. Fields defined by solid line in (f) and (g) are referred to clinopyroxenes composition in harzburgites and lherzolites from Tres Lagos and Las Cumbres; fields defined by dotted line in (f) and (g) are referred to clinopyroxenes composition in harzburgites and lherzolites from Cerro Fraile and Pali Aike. Data from Aliani et al. (2009), Bjerg et al. (2005, 2009), Conceicao et al. (2005),; Dantas (2007), Dantas et al. (2009), Faccini et al. (2013), Gorring and Kay (2000), Kilian and Stern (2002), Laurora et al. (2001), Melchiorre et al. (2015), Mundl et al. (2015, 2016), Ntaflos et al. (2007), Rivalenti et al. (2004, 2007), Schilling et al. (2005, 2008, 2017), and Stern et al. (1999). See also text and Table 2.

Table 1

Sr-Nd isotopic signature of clinopyroxene separates from representative Patagonian mantle xenoliths. The trace element composition (ppm) of the selected clinopyroxene are from Aliani et al. (2009), Dantas (2007), Dantas et al. (2009), Faccini et al. (2013) and Melchiorre et al. (2015).

Locality	Sample	Rb	Sr	1/Sr	$^{87}Rb/^{86}Sr$	$^{87}Sr/^{86}Sr$	2σ	Sm	Nd	1/Nd	$^{147}Sm/^{144}Nd$	$^{143}Nd/^{144}Nd$	2σ	La	Ce	Nd	Sm	Eu	Gd	Dy	Er	Yb	Lu
Cerro Rio Chubut	CH 8	n.m.	n.m.	-	-	0.703873	0.000008	n.m.	n.m.	-	-	0.512902	0.000016	n.m.	n.m.	n.m.	n.m.	n.m.	n.m.	n.m.	n.m.	n.m.	n.m.
Cerro de los Chenques	PM 12-12	0.49	62.1	0.016	0.023001	0.702736	0.000009	1.84	4.30	0.232	0.258362	0.513038	0.000018	0.89	3.67	4.30	1.84	0.71	2.85	3.67	2.37	1.96	0.32
	PM 12-13	0.45	67.9	0.015	0.018964	0.703417	0.000011	1.42	3.66	0.274	0.233496	0.512848	0.000020	0.90	3.06	3.66	1.42	0.57	2.16	3.15	2.18	2.02	0.30
	PM 12-15	0.56	68.2	0.015	0.023748	0.703463	0.000008	1.01	2.94	0.341	0.207552	0.51289	0.000006	0.78	2.83	2.94	1.01	0.48	2.07	3.11	2.30	2.68	0.29
	PM 12-17	0.60	99.1	0.010	0.017427	0.704077	0.000011	2.04	4.22	0.237	0.291797	0.512723	0.000022	0.90	3.38	4.22	2.04	0.87	3.30	3.95	2.69	2.49	0.41
	PM 12-19	0.67	73.9	0.014	0.026213	0.702704	0.000011	1.98	4.88	0.205	0.244851	0.513087	0.000011	1.26	3.78	4.88	1.98	0.76	2.29	3.98	2.54	2.23	0.33
	PM 12-26	0.93	88.5	0.011	0.030411	0.703696	0.000008	0.97	4.14	0.242	0.141309	0.512734	0.000009	0.68	2.93	4.14	0.97	0.30	0.85	0.68	0.37	0.54	0.10
	PM 12-48	0.54	84.9	0.012	0.018521	0.703988	0.000009	1.44	4.26	0.235	0.203867	0.512696	0.000011	1.21	3.00	4.26	1.44	0.47	1.68	3.11	2.29	1.67	0.28
Cerro Clark	PM 24-22	0.10	45.7	0.022	0.006400	0.703432	0.000009	1.53	3.80	0.264	0.242365	0.512867	0.000007	0.99	3.43	3.80	1.53	0.64	2.29	2.88	2.06	1.87	0.26
	PM 24-27	0.17	186	0.005	0.002673	0.703236	0.000010	2.21	9.76	0.102	0.136262	0.512915	0.000010	9.28	19.1	9.76	2.21	0.79	2.38	2.74	1.50	1.50	0.22
	PM 24-32	0.30	66.6	0.015	0.012819	0.704297	0.000009	1.16	3.26	0.307	0.214308	0.512772	0.000011	1.25	3.75	3.26	1.16	0.48	1.56	2.02	1.24	1.26	0.15
Estancia Sol de Mayo	MGP 1-A	n.m.	138	0.007	-	0.703859	0.000009	2.37	9.11	0.110	0.156623	0.512756	0.000010	6.18	15.8	9.11	2.37	0.65	1.87	1.99	1.34	1.65	0.33
	MGP 2-A	n.m.	99.0	0.010	-	0.703706	0.000009	1.37	4.92	0.203	0.168113	0.512791	0.000022	3.74	8.37	4.92	1.37	0.44	1.41	1.55	0.82	0.80	0.15
	MGP 2-B	n.m.	100	0.010	-	0.703743	0.000009	1.70	5.81	0.172	0.175953	0.512787	0.000012	3.81	9.13	5.81	1.70	0.59	1.95	2.26	1.40	1.39	0.21
	MGP 4-A	n.m.	125	0.008	-	0.703676	0.000009	2.97	11.2	0.089	0.160217	0.512694	0.000032	5.36	16.6	11.2	2.97	0.94	2.80	2.99	1.57	1.38	0.21
Gobernador Gregores	PM 23-1	0.22	258	0.004	0.002466	0.703073	0.000013	6.90	23.8	0.042	0.174639	0.512904	0.000007	8.23	26.7	23.8	6.90	2.19	6.53	4.45	1.45	b.d.l.	0.07
	PM 23-6	0.21	444	0.002	0.001391	0.703046	0.000009	9.59	36.0	0.028	0.160854	0.512947	0.000009	29.2	57.5	36.0	9.59	3.02	8.60	5.58	1.61	b.d.l.	0.10
	PM 23-16	0.10	452	0.002	0.000611	0.703128	0.000011	8.16	37.3	0.027	0.132006	0.512865	0.000011	21.8	56.2	37.3	8.16	2.45	6.75	4.46	1.94	b.d.l.	0.24
	DUB 1g_1	n.m.	194	0.005		0.703259	0.000007	2.90	13.3	0.075	0.131510	0.512872	0.000005	17.3	23.3	13.3	2.90	1.14	3.47	2.36	1.12	0.88	b.d.l.
	DUB 1g_2	n.m.	333	0.003	-	0.703245	0.000009	5.29	24.1	0.041	0.132169	0.512866	0.000006	10.6	32.7	24.1	5.29	1.28	3.80	2.57	0.800	0.79	b.d.l.
	DUB 2g	n.m.	234	0.004	-	0.703345	0.000010	7.43	27.8	0.036	0.161021	0.512807	0.000005	9.75	34.0	27.8	7.43	2.10	6.27	3.90	1.63	0.98	b.d.l.
Cerro Fraile	CF 6A	n.m.	21.3	0.047	-	0.703416	0.000007	0.77	2.71	0.369	0.171525	0.512922	0.000024	6.17	9.54	2.71	0.77	0.21	0.52	0.49	0.38	0.45	0.08
	CF 8	n.m.	n.m.	-	-	0.703351	0.000013	n.m.	n.m.	-	-	-	-	n.m.	n.m.	n.m.	n.m.	n.m.	n.m.	n.m.	n.m.	n.m.	n.m.
	CF 13	n.m.	n.m.	-	-	0.703232	0.000009	n.m.	n.m.	-	-	0.512886	0.000017	n.m.	n.m.	n.m.	n.m.	n.m.	n.m.	n.m.	n.m.	n.m.	n.m.
Pali Aike	PA 1	n.m.	n.m.	-	-	0.703246	0.000008	n.m.	n.m.	-	-	0.512911	0.000001	n.m.	n.m.	n.m.	n.m.	n.m.	n.m.	n.m.	n.m.	n.m.	n.m.
	PA 2	n.m.	n.m.	-	-	0.703197	0.000010	n.m.	n.m.	-	-	0.51284	0.000008	n.m.	n.m.	n.m.	n.m.	n.m.	n.m.	n.m.	n.m.	n.m.	n.m.

PA 5	n.m.	n.m.	-	-	0.703338	0.000010	n.m.	n.m.	-	-	0.512894	0.000009	n.m.	n.m.	n.m.	n.m.	n.m.	n.m.	n.m.	n.m.	n.m.	n.m.
PA 8	n.m.	n.m.	-	-	0.703216	0.000010	n.m.	n.m.	-	-	0.512986	0.000009	n.m.	n.m.	n.m.	n.m.	n.m.	n.m.	n.m.	n.m.	n.m.	n.m.
PA 13	n.m.	n.m.	-	-	0.703464	0.000010	n.m.	n.m.	-	-	0.512939	0.000012	n.m.	n.m.	n.m.	n.m.	n.m.	n.m.	n.m.	n.m.	n.m.	n.m.

n.m. = not measured; b.d.l. = below detection limit

Table 2

Summary of the main geochemical features of the Northern, Central and Southern Patagonia mantle xenoliths. The latitude (°S), longitude (°W), distance from trench (km), age of the xenoliths-bearing host rock (Ma) and xenoliths type are listed for each Patagonian locality, together with the identification number reported in Fig. 1. Additionally, Re-Os (T_{RD}) ages, calculated partial melting degrees (F%) experienced by orthopyroxene and clinopyroxene, and forsterite (Fo) content of olivine are also shown. Partial melting degrees and olivine Fo ranges are calculated/reported only for harzburgites and lherzolites. Sp = spinel; Grt = garnet; Cpx = clinopyroxene; Opx = orthopyroxene; Ol = olivine. Hz = harzburgite; Lh = lherzolite; Du = dunite; Wh = wehrlite; Wb = websterite; Opxite = orthopyroxenite; Cpxite = clinopyroxenite. * indicates values calculated only on spinel-bearing lherzolites and harzburgites.

Locality (Number in Fig. 1)	Latitude (°S)	Longitude (°W)	Distance from trench (km)	Type of xenoliths	Host rock age (Ma)	Xenoliths T_{RD} age (Ga)	F(%) from Opx major elements	F(%) from Cpx major elements	F(%) from Cpx trace elements	Fo (Ol)	References
Northern Patagonia (39/40°-46°)											
Laguna Fria (**1**)	40° 21'	68° 38'	546	Sp-Hz	1-5	-	-	-	-	90.8	Bjerg et al. (2005)
Cerro Chenque (**2**)	40° 29'	68° 44'	537	Sp-Hz; Du	-	0.5-1	23-31	18	14	91.0-91.9	Mundl et al. (2016)
Puesto Diaz (**3**)	40° 30'	68° 44'	537	Sp-Hz; Du	-	0.7-1	2[illegible]0	18-21	7-17	90.8-91.8	Mundl et al. (2016)
Estancia Alvarez (**4**)	40° 46'	68° 45'	531	Sp-Lh; Sp-Hz	-	-	[illegible]0	-	-	90.0-90.5	Rivalenti et al. (2004)
Cerro Aznares (**5**)	40° 48'	68° 41'	540	Wb	20-29	-	-	-	-	89.5-91.0	Dantas (2007)
Comallo (**6**)	40° 55'	69° 52'	437	Sp-Hz	1-2	0.6-1[illegible]	[illegible]1-27	17-20	7-13	91.1-91.9	Mundl et al. (2016)
Cerro Mojon (**7**)	41° 06'	70° 13'	415	Sp-Lh; Sp-Hz; Du	-	-	-	18-20	6-15	91.0-91.5	Conceicao et al. (2005); Rivalenti et al. (2004)
Prahuaniyeu (**8**)	41° 20'	67° 54'	613	Sp-Lh; Sp-Hz; Sp-Wb; Sp+G[illegible]-Lh; G[illegible]-Lh	[illegible]0-2[illegible]	0.6-1.7	10-23*	7-25*	6-20*	89.2-91.7	Bjerg et al. (2009); Dantas (2007); Mundl et al. (2016)
Traful (**9**)	41° 38'	69° 18'	497	S[illegible]-Hz	23-25	-	-	-	-	91.6	Bjerg et al. (2005)
Cerro Rio Chubut (**10**)	43° 38'	68° 58'	53[illegible]	Sp[illegible]h; Sp-Hz; Sp-Wb; Wb	49-52	-	11-30	6-17	1-10	89.5-92.0	Dantas (2007); This work
Paso de los Indios (**11**)	43° 48'	68° 55'	5[illegible]6	Sp-Lh; Sp-Hz	23-34	-	-	17-21	13-14	90.0-91.5	Rivalenti et al. (2004)
Cerro de los Chenques (**12**)	44° 52'	[illegible]° 04	456	Sp-Lh; Sp-Hz; Du; Sp-Wb	20-25	-	14-27	10-22	3-15	88.8-91.4	Dantas (2007); Dantas et al. (2009); Rivalenti et al. (2004, 2007); This work
Coyhaique (**13**)	[illegible]° 35'	[illegible]2° 08'	300	Sp-Lh	57-61	1.31-1.7	27-30	-	-	91.2-91.5	Schilling et al. (2017)
Central Patagonia (46°-49°)											
Chile Chico (**14**)	46° 34	71° 46'	306	Sp-Lh	39-42	0.81-0.88	23-26	10	-	90.0-90.3	Schilling et al. (2017)
Cerro Clark (**15**)	46° 43'	69° 29'	476	Sp-Lh; Sp-Wb; Sp-Cpxite; Cpxite	11-12	0.78-0.82	12-17	10-17	2-8	89.0-90.7	Dantas (2007); Dantas et al. (2009); Schilling et al. (2017); This work
Estancia Sol de Mayo (**16**)	46° 49'	71° 25'	326	Sp-Lh; Sp-Hz; Du; Wh	2-7	-	19-30	17-21	-	88.1-91.8	Melchiorre et al. (2015); This work
Don Camilo (**17**)	46° 59'	68° 32'	552	Sp-Lh; Sp-Hz	0-5	0.9	-	12-17	3-7	-	Mundl et al. (2015)
Cerro Cuadrado (**18**)	48° 07'	70° 08'	474	Sp-Lh; Sp-Hz	-	-	13-24	12-16	1-8	89.6-91.3	Rivalenti et al. (2004)
Auvernia (**19**)	48° 27'	68° 10'	625	Sp-Lh; Sp-Hz	0-1	1.59-2.13	22-27	13-15	-	91.1-91.7	Schilling et al. (2017)
Gobernador Gregores (**20**)	48° 34'	70° 10'	487	Sp-Lh; Sp-Hz; Wh; Wb	3-4	0.5-1.86	8-31	3-22	3-17	87.5-92.1	Aliani et al. (2009); Conceicao et al. (2005); Dantas (2007); Gorring

Cerro Redondo (**21**)	48° 59'	70° 10'	495	Sp-Lh; Sp-Hz	-	-	15-24	8-22	-	90.3-91.5	and Kay (2000); Laurora et al. (2001); Mundl et al. (2015); Rivalenti et al. (2004); This work Conceicao et al. (2005); Schilling et al. (2005)
Southern Patagonia (49°-54°)											
Tres Lagos (**22**)	49° 11'	71° 20'	412	Sp-Lh; Sp-Hz; Du	4-7	0.6-2.0	10-30	9-19	1-14	88.9-91.3	Mundl et al. (2015); Ntaflos et al. (2007); Rivalenti et al. (2004)
Cerro Fraile (**23**)	50° 33'	72° 38'	284	Sp-Lh; Sp-Hz; Du; Cpxite; Opxite	1-2	0.81-2.04	12-[illegible]	12-23	4-21	88.0-91.0	Faccini et al. (2013); Rivalenti et al. (2004); This work
Las Cumbres (**24**)	50° 42'	72° 20'	304	Sp-Lh; Sp-Hz; Du	-	-	17-25	17-18	5-12	88.4-89.8	Rivalenti et al. (2004)
Pali Aike (**25**)	52° 01'	70° 09'	406	Sp-Lh; Sp-Hz; Sp+Grt-Lh; Grt-Lh; Grt-Hz	0-3	0.[illegible]2.5	12-18*	7-25*	2-24*	87.9-90.7	Dantas (2007); Mundl et al. (2015); This work

Highlights

Southern Patagonia mantle experienced lower partial melting degrees in older times

Refertilization and metasomatic processes occurred in Patagonia lithospheric mantle

Enrichment processes were intimately related to the uprising back-arc plateau lavas

Pyroxenites record infiltration of tholeiitic and alkaline melts within the mantle

Declaration of interests

☒ The authors declare that they have no known competing financial interests or personal relationships that could have appeared to influence the work reported in this paper.

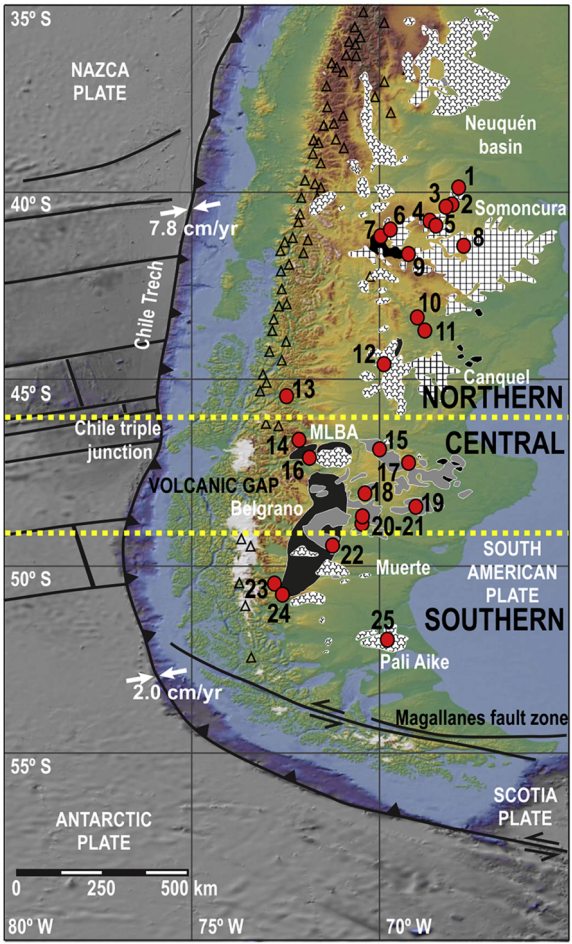
35° S
NAZCA PLATE
Neuquén basin
40° S
7.8 cm/yr
Somoncura
Chile Trech
45° S
Canquel
NORTHERN
Chile triple junction
MLBA
CENTRAL
VOLCANIC GAP
Belgrano
SOUTH AMERICAN PLATE
50° S
Muerte
SOUTHERN
Pali Aike
2.0 cm/yr
Magallanes fault zone
55° S
SCOTIA PLATE
ANTARCTIC PLATE
0 250 500 km
80° W
75° W
70° W
Eocene
Holocene to Pliocene
Early Miocene to Oligocene
Volcanoes
Pliocene to late Miocene
Mantle xenoliths localities

Figure 1

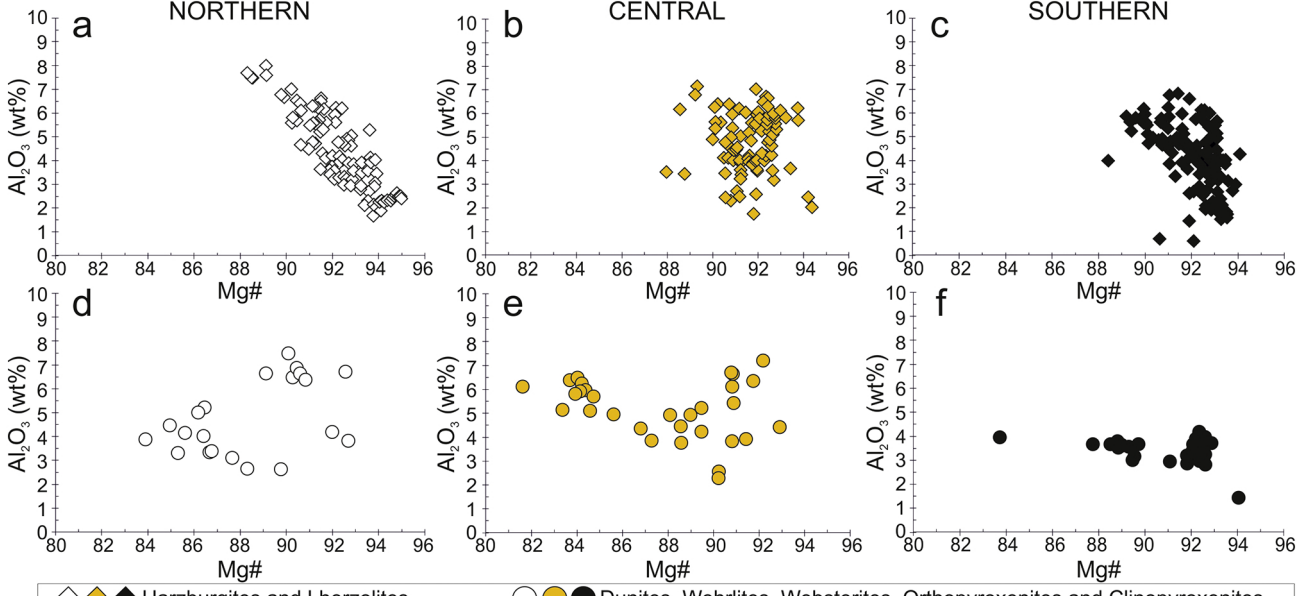
a
NORTHERN
b
CENTRAL
c
SOUTHERN
d
e
f
Al2O3 (wt%)
Mg#
Harzburgites and Lherzolites
Dunites, Wehrlites, Websterites, Orthopyroxenites and Clinopyroxenites

Figure 2

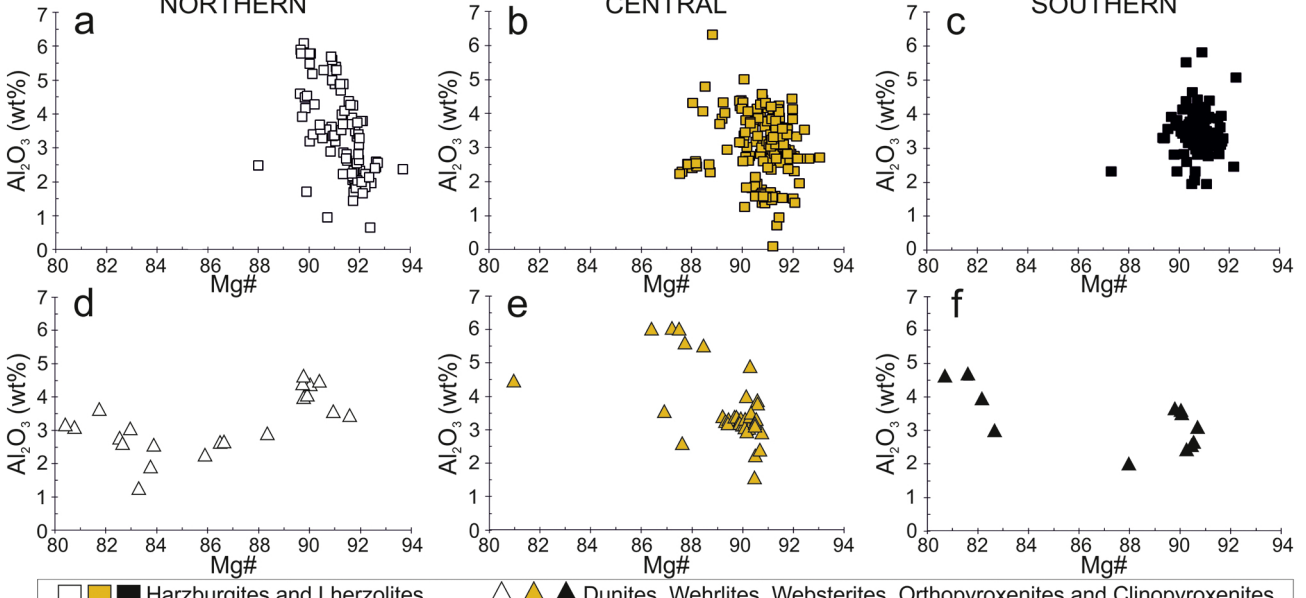
NORTHERN
CENTRAL
SOUTHERN
a
b
c
d
e
f
Al2O3 (wt%)
Mg#
Harzburgites and Lherzolites
Dunites, Wehrlites, Websterites, Orthopyroxenites and Clinopyroxenites

Figure 3

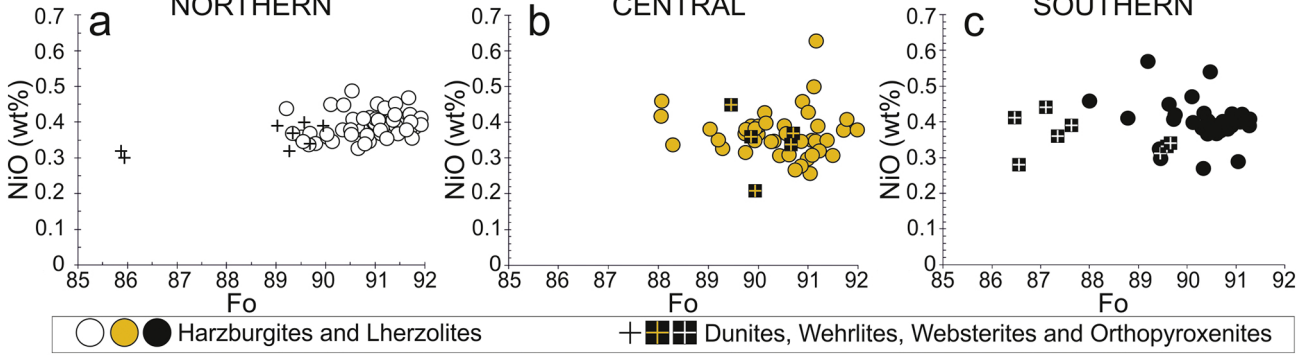
a
NORTHERN
b
CENTRAL
c
SOUTHERN
NiO (wt%)
Fo
0.7
0.6
0.5
0.4
0.3
0.2
0.1
0
85
86
87
88
89
90
91
92
Harzburgites and Lherzolites
Dunites, Wehrlites, Websterites and Orthopyroxenites

Figure 4

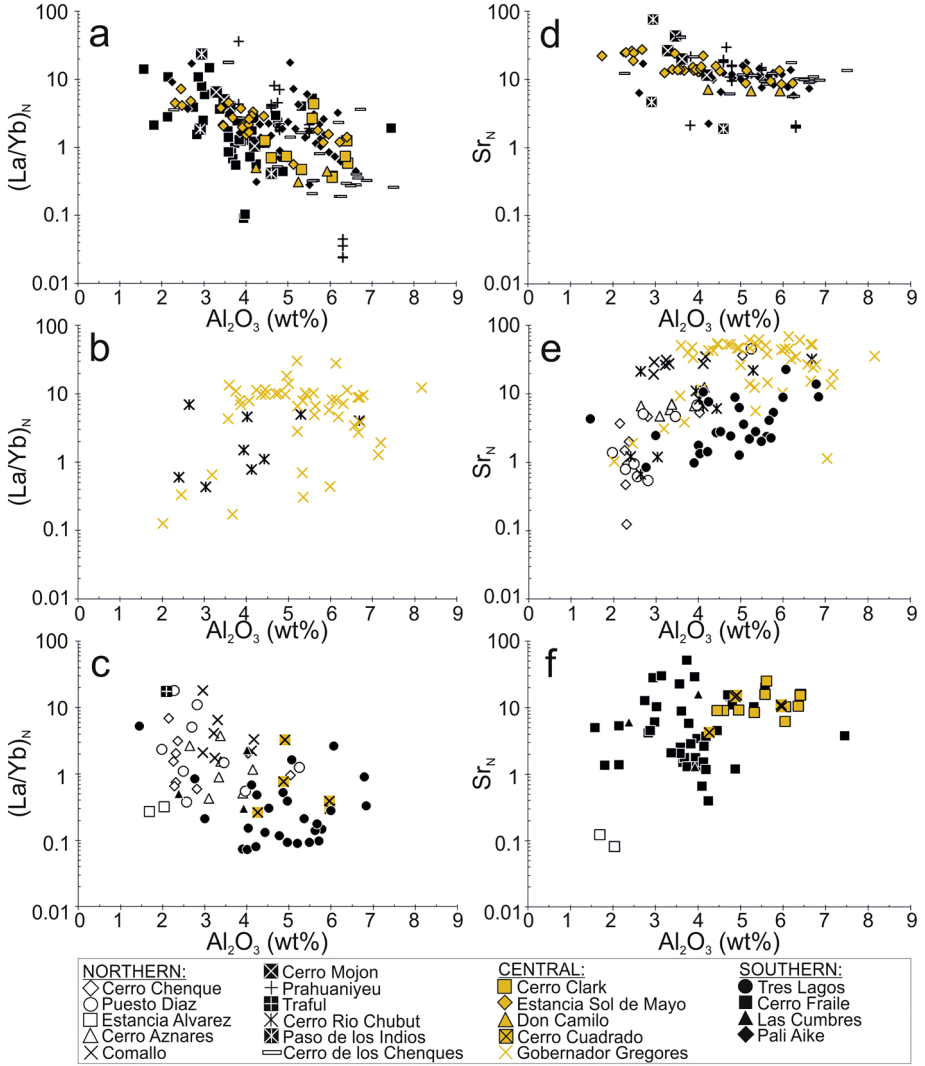
a
b
c
d
e
f
(La/Yb)N
SrN
Al2O3 (wt%)
NORTHERN:
Cerro Chenque
Puesto Diaz
Estancia Alvarez
Cerro Aznares
Comallo
Cerro Mojon
Prahuaniyeu
Traful
Cerro Rio Chubut
Paso de los Indios
Cerro de los Chenques
CENTRAL:
Cerro Clark
Estancia Sol de Mayo
Don Camilo
Cerro Cuadrado
Gobernador Gregores
SOUTHERN:
Tres Lagos
Cerro Fraile
Las Cumbres
Pali Aike

Figure 5

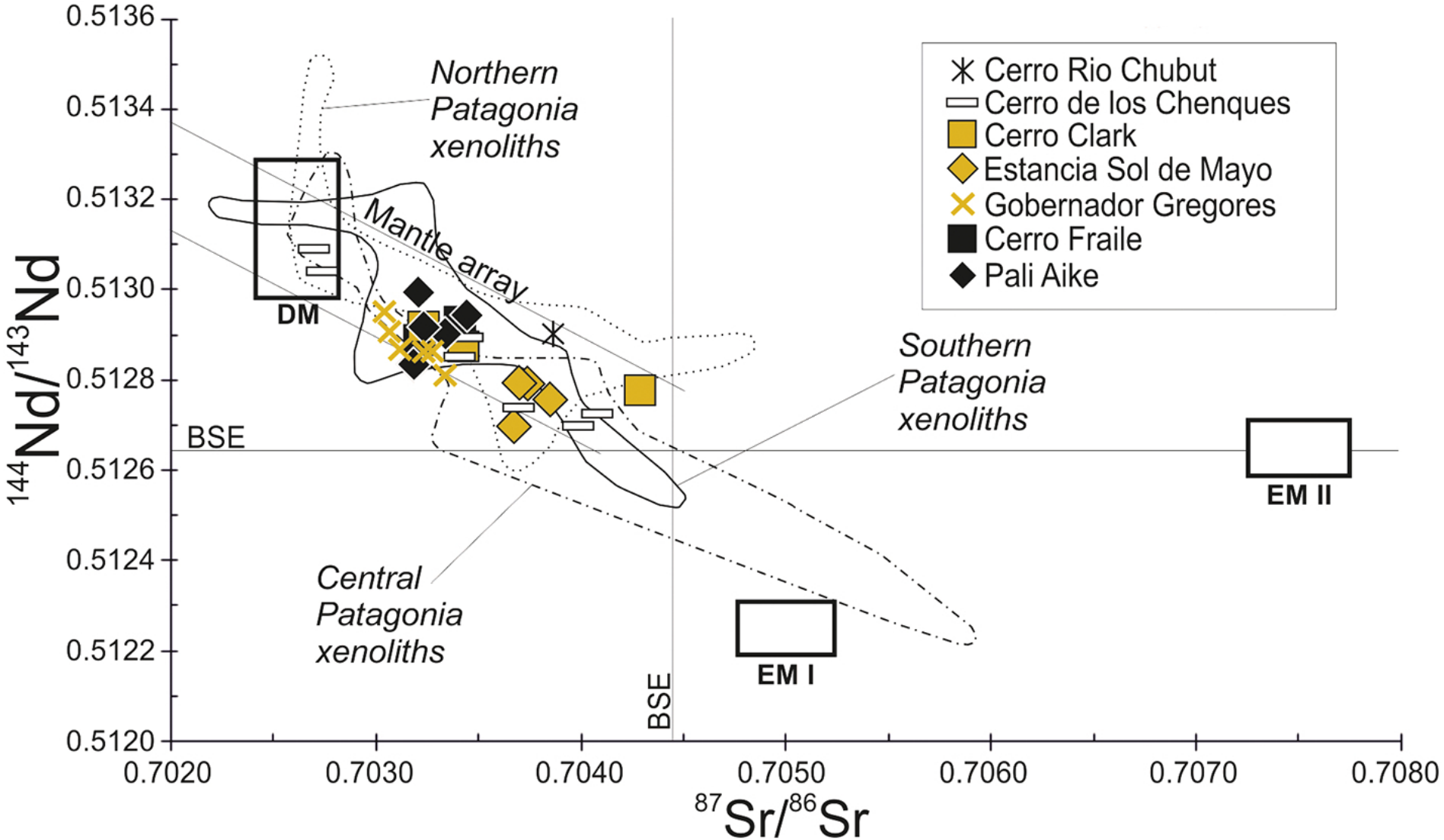
Cerro Rio Chubut
Cerro de los Chenques
Cerro Clark
Estancia Sol de Mayo
Gobernador Gregores
Cerro Fraile
Pali Aike
Northern Patagonia xenoliths
Mantle array
Southern Patagonia xenoliths
Central Patagonia xenoliths
DM
EM II
EM I
BSE
BSE
0.5136
0.5134
0.5132
0.5130
0.5128
0.5126
0.5124
0.5122
0.5120
0.7020
0.7030
0.7040
0.7050
0.7060
0.7070
0.7080
144Nd/143Nd
87Sr/86Sr

Figure 6

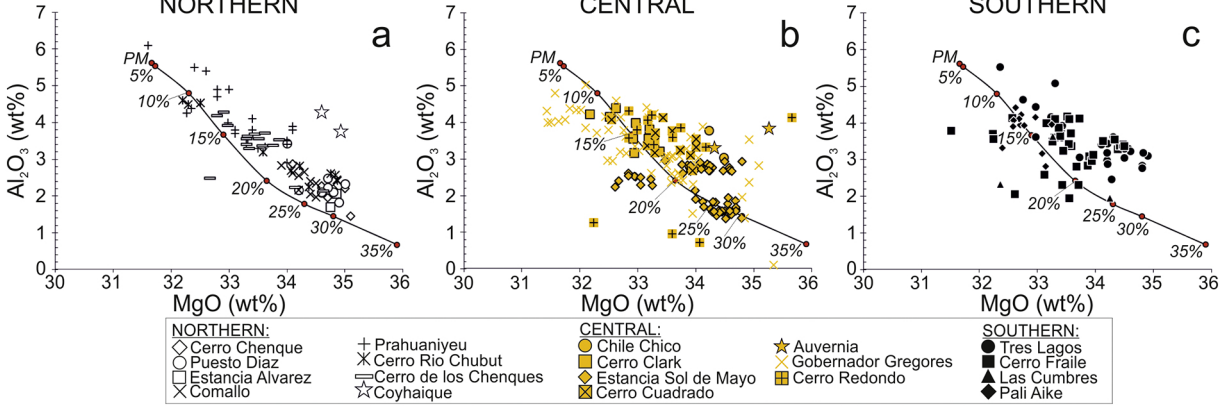
NORTHERN
a
CENTRAL
b
SOUTHERN
c
Al2O3 (wt%)
MgO (wt%)
PM
5%
10%
15%
20%
25%
30%
35%
NORTHERN:
Cerro Chenque
Puesto Diaz
Estancia Alvarez
Comallo
Prahuaniyeu
Cerro Rio Chubut
Cerro de los Chenques
Coyhaique
CENTRAL:
Chile Chico
Cerro Clark
Estancia Sol de Mayo
Cerro Cuadrado
Auvernia
Gobernador Gregores
Cerro Redondo
SOUTHERN:
Tres Lagos
Cerro Fraile
Las Cumbres
Pali Aike

Figure 7

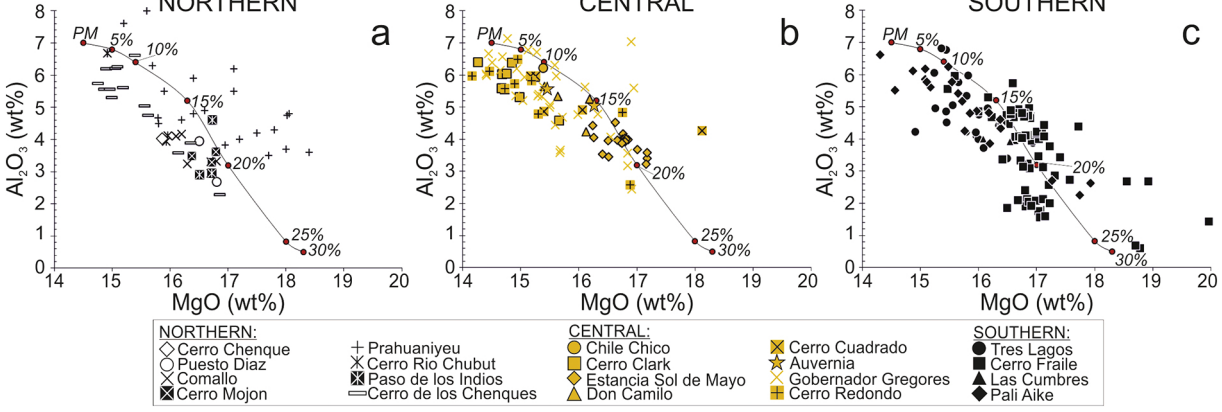
NORTHERN
a
CENTRAL
b
SOUTHERN
c
PM
5%
10%
15%
20%
25%
30%
Al2O3 (wt%)
MgO (wt%)
NORTHERN:
Cerro Chenque
Puesto Diaz
Comallo
Cerro Mojon
Prahuaniyeu
Cerro Rio Chubut
Paso de los Indios
Cerro de los Chenques
CENTRAL:
Chile Chico
Cerro Clark
Estancia Sol de Mayo
Don Camilo
Cerro Cuadrado
Auvernia
Gobernador Gregores
Cerro Redondo
SOUTHERN:
Tres Lagos
Cerro Fraile
Las Cumbres
Pali Aike

Figure 8

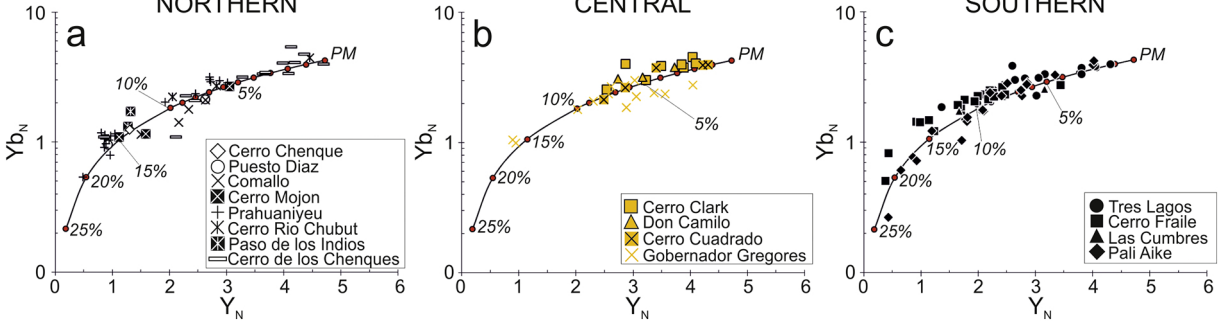
NORTHERN
a
PM
10%
5%
15%
20%
25%
Cerro Chenque
Puesto Diaz
Comallo
Cerro Mojon
Prahuaniyeu
Cerro Rio Chubut
Paso de los Indios
Cerro de los Chenques
CENTRAL
b
PM
10%
5%
15%
20%
25%
Cerro Clark
Don Camilo
Cerro Cuadrado
Gobernador Gregores
SOUTHERN
c
PM
5%
15%
10%
20%
25%
Tres Lagos
Cerro Fraile
Las Cumbres
Pali Aike
Yb$_N$
Y$_N$
0
1
2
3
4
5
6
10

Figure 9

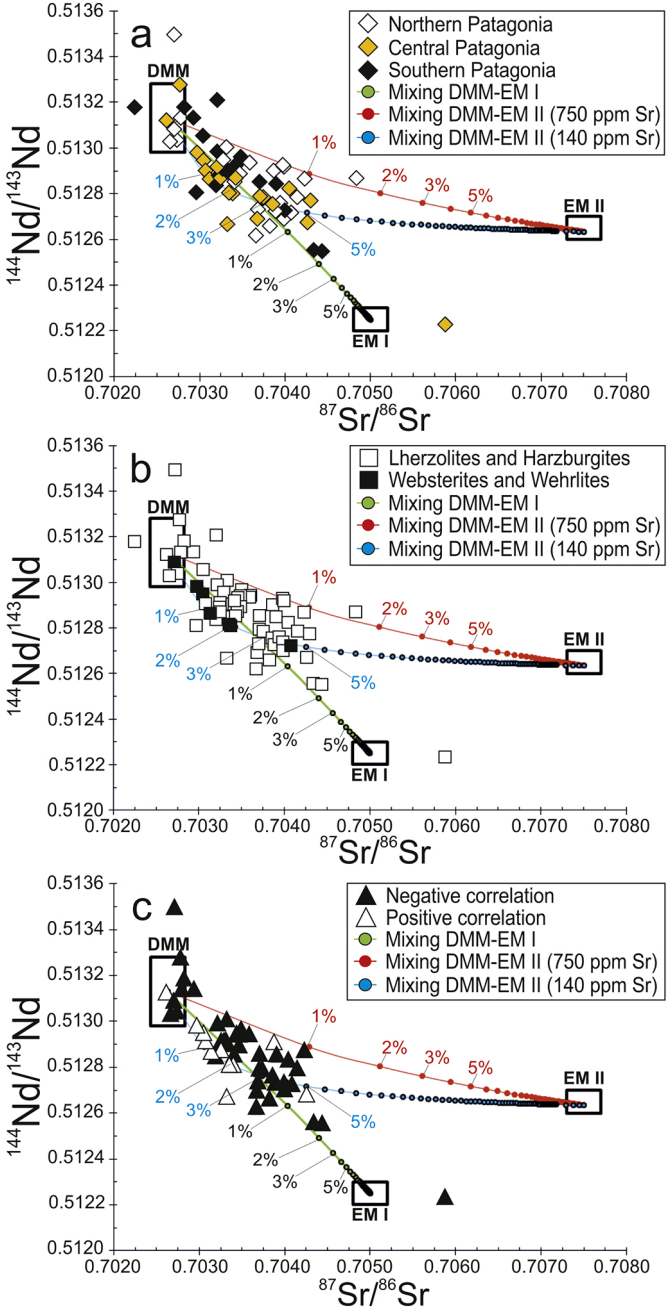
a
Northern Patagonia
Central Patagonia
Southern Patagonia
Mixing DMM-EM I
Mixing DMM-EM II (750 ppm Sr)
Mixing DMM-EM II (140 ppm Sr)
DMM
EM II
EM I
1%
2%
3%
5%
$^{144}Nd/^{143}Nd$
$^{87}Sr/^{86}Sr$
0.5136
0.5134
0.5132
0.5130
0.5128
0.5126
0.5124
0.5122
0.5120
0.7020
0.7030
0.7040
0.7050
0.7060
0.7070
0.7080
b
Lherzolites and Harzburgites
Websterites and Wehrlites
Mixing DMM-EM I
Mixing DMM-EM II (750 ppm Sr)
Mixing DMM-EM II (140 ppm Sr)
DMM
EM II
EM I
c
Negative correlation
Positive correlation
Mixing DMM-EM I
Mixing DMM-EM II (750 ppm Sr)
Mixing DMM-EM II (140 ppm Sr)
DMM
EM II
EM I

Figure 10

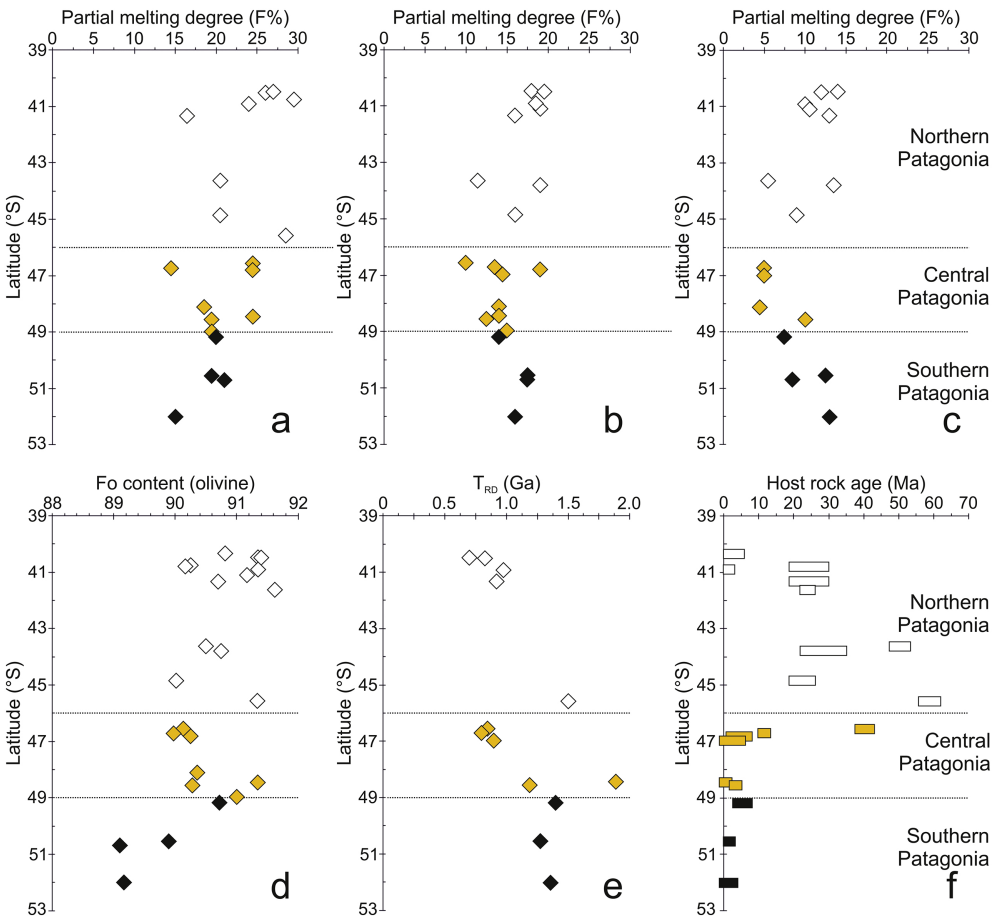
Partial melting degree (F%)
0 5 10 15 20 25 30
Latitude (°S)
39 41 43 45 47 49 51 53
a
b
c
Northern Patagonia
Central Patagonia
Southern Patagonia
Fo content (olivine)
88 89 90 91 92
T_{RD} (Ga)
0 0.5 1.0 1.5 2.0
Host rock age (Ma)
0 10 20 30 40 50 60 70
d
e
f

Figure 11

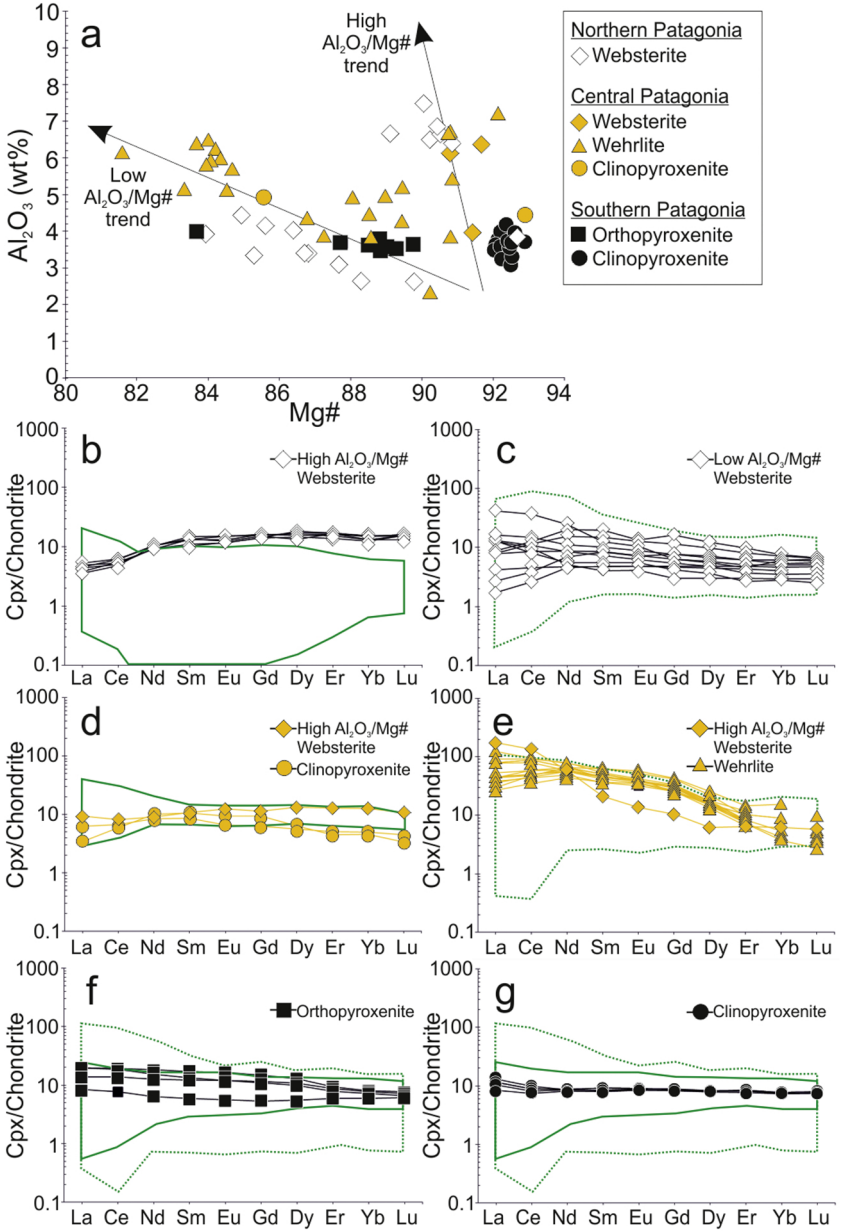
a
High Al2O3/Mg# trend
Low Al2O3/Mg# trend
Al2O3 (wt%)
Mg#
Northern Patagonia
Websterite
Central Patagonia
Websterite
Wehrlite
Clinopyroxenite
Southern Patagonia
Orthopyroxenite
Clinopyroxenite
b
High Al2O3/Mg# Websterite
c
Low Al2O3/Mg# Websterite
d
High Al2O3/Mg# Websterite
Clinopyroxenite
e
High Al2O3/Mg# Websterite
Wehrlite
f
Orthopyroxenite
g
Clinopyroxenite
Cpx/Chondrite
La Ce Nd Sm Eu Gd Dy Er Yb Lu

Figure 12